JGR Solid Earth

RESEARCH ARTICLE
10.1029/2019JB018561

Special Section:
Creep on continental faults and subduction zones: Geophysics, geology, and mechanics

Probing the Variation in Aseismic Slip Behavior Around an Active Suture Zone: Observations of Repeating Earthquakes in Eastern Taiwan

Yaochieh Chen[1,2], Kate Huihsuan Chen[1], Jyr-Ching Hu[3], and Jian-Cheng Lee[4]

[1]Department of Earth Sciences, National Taiwan Normal University, Taipei, Taiwan, [2]Institut des Sciences de la Terre (ISTerre), Université Grenoble Alpes, Grenoble, France, [3]Department of Geosciences, National Taiwan University, Taipei, Taiwan, [4]Institue of Earth Sciences, Academia Sinica, Taipei, Taiwan

Key Points:
- Using 202 M_L 2.0 to 4.6 repeating earthquake sequences from 2000 to 2011, we studied where and how faults creep in an active suture zone
- An unexpected high creep rate of 4.3 cm/year is found to occur along the 80-km-long Central Range fault
- The time-dependent aseismic slip showed a strong correlation with the creepmeter data, suggesting a common mechanism

Supporting Information:
- Supporting Information S1

Correspondence to:
K. H. Chen,
katepili@gmail.com

Citation:
Chen, Y., Chen, K. H., Hu, J.-C., & Lee, J.-C. (2020). Probing the variation in aseismic slip behavior around an active suture zone: Observations of repeating earthquakes in eastern Taiwan. *Journal of Geophysical Research: Solid Earth*, *124*;e2019JB018561. https://doi.org/10.1029/2019JB018561

Received 19 AUG 2019
Accepted 13 APR 2020
Accepted article online 20 APR 2020

Abstract An examination of repeating earthquakes in eastern Taiwan revealed previously unrecognized quasiperiodic repetition of aseismic creep along two reverse faults in an active suture zone. Using 202 M_L 2.0 to 4.6 repeating earthquake sequences (RES) during the period from 2000 to 2011, we studied where and how certain faults creep. The RES were found to be highly concentrated in the southern segment of the Longitudinal Valley fault (LVF) and in the northern segment of the Central Range fault (CRF). They are mainly located at a depth of 10–25 km and show strong regional differences in creep behavior. Using the moment release rate of RES and geodetically derived long-term slip rate, we re-estimate the empirical relationship between deep creep and seismic moment for creeping sections in eastern Taiwan. For the 30-km-long LVF, the creep rate increased dramatically from 1.5 to 12.3 cm/year under the influence of the M_L 6.4 Chengkung earthquake of 2003. For the 80-km-long CRF, the high creep rate of 4.3 cm/year appears to have been stable over time and is descriptive of a previously unrecognized deep structure underneath the eastern flank of the Central Range. The quasiperiodic pulsing of the deep slip rate has a predominant interval of 1 year for both segments. After the M_L 6.4 event, the predominant interval for the creeping LVF halved in duration. The time-dependent aseismic slip showed a strong correlation with the creepmeter data, suggesting that the positing of a common mechanism is needed to connect the surface and deep creep variation.

1. Introduction

Fault creep on strike-slip faults has been fairly well documented in tectonically active continental regions, but there are few studies on creeping thrust and normal faults (Harris, 2017). The lack of attention paid to creep on dip-slip faults has meant that the nature of fault creep and its role in large earthquake generation remain unknown. The creeping sections of the Longitudinal Valley fault (LVF) in Taiwan serve as one of the best examples of faults that rapidly creep at the surface, and it is also known to have produced several major earthquakes ($M_L \geq 6$) over the past 100 years.

The Central Range of Taiwan developed around 6–5 Ma due to the ongoing arc-continental collision between the Philippine Sea and Eurasian plates and behaves as an active orogenic belt (Liu et al., 2000). The N-S trending Longitudinal Valley in eastern Taiwan is the suture between the colliding volcanic arc (Coastal Range) and the mountainous backbone of Taiwan (Central Range). To the east, the valley is bounded by the Coastal Range along the LVF, and to the west, the valley is bounded by the Central Range along the Central Range fault (CRF). The east-dipping, oblique-slip LVF that is responsible for a horizontal velocity of 3–4 cm/year (Angelier et al., 1997; Hsu & Bürgmann, 2006; Lee et al., 2001; Yu & Kuo, 2001; Yu & Liu, 1989; Yu et al., 1990) is where the most destructive seismic episode ever known in eastern Taiwan occurred in 1951. This 1951 M_L 7.3 Hualien-Taitung sequence is composed of three M_L 7 events and 12 M_L 6 events that shocked eastern Taiwan. From 21 October to 5 December, the sequence caused sequential ruptures along four distinct segments (Cheng et al., 1996; Hsu, 1962), suggesting that the heterogeneous fault properties may influence the generation of large earthquakes.

The LVF can be subdivided into four segments from north to south based on their structural, stratigraphic, and seismic characteristics. These segments are the Linding, Ruisui, Chihshang, and Lichi faults (Chen, Yen, et al., 2007), as represented by the pink lines in Figure 1. The CRF that is responsible

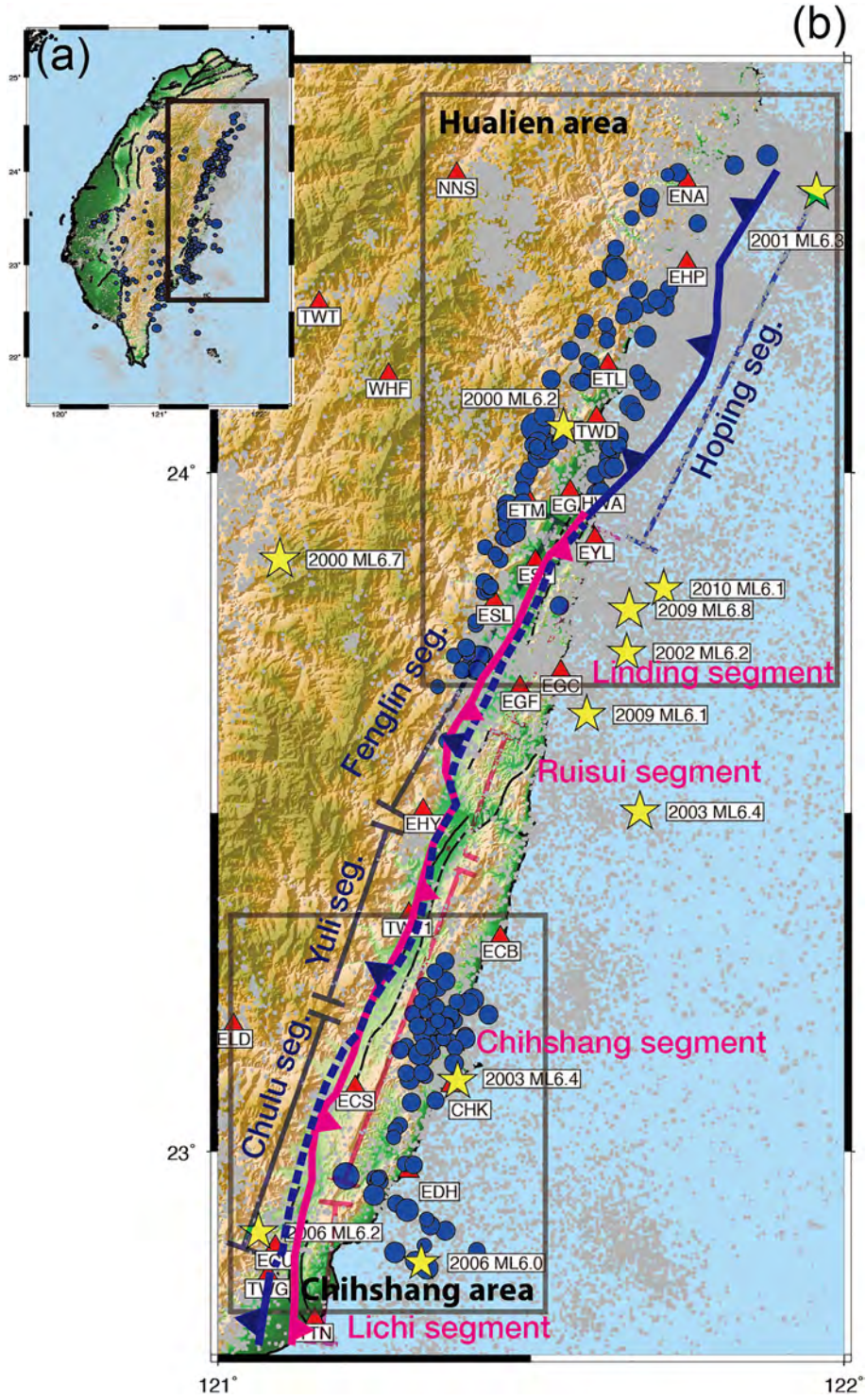

Figure 1. (a) Map of Taiwan and the study area. Location of background seismicity and the $M_L \geq 2$ repeating earthquake sequences (RES) during the study period of 2000 to 2011 are denoted by gray dots and blue circles, respectively. (b) Close-up view of the RES in the Longitudinal Valley area (blue circles), background seismicity (gray circles), and $M_L \geq 6$ earthquakes (yellow stars). Blue and pink lines indicate the Central Range fault (CRF) and Longitudinal Valley fault (LVF) separately. Segmentation of the LVF and CRF is from Chen, Nadeau, and Rau (2007), Chen, Yen, et al. (2007), and Chen et al. (2018), respectively, where the dashed lines indicate the blind faults or no clear surface rupture.

for the 1- to 2-cm/year uplift rate of the mountain (Ching et al., 2011; Ching, Rau, & Zeng, 2007; Ching, Rau, Lee, & Hu, 2007; Rau et al., 2008; Yu et al., 1997) was the site of the 2013 M_L 6.4 Ruisui and the 2014 M_L 5.9 Fenglin earthquakes and has been inferred to be a west-dipping blind fault (Biq, 1965; Canitano et al., 2015; Chuang et al., 2014; Lee et al., 2014; Shyu et al., 2006; Wen et al., 2016; Wu et al., 2006). The western digging fault was also inferred to correspond to the 2018 Hualien events (Tung et al., 2019; Yen et al., 2019). Based on the findings of past geological and seismological investigations, the CRF can be subdivided into five segments from north to south: Hoping, Fenglin, Yuli, Chulu, and Binlang segments (Chen et al., 2018), as indicated by the blue lines in Figure 1. Note that the southernmost part of CRF (Binlang) is located outside the mapped area. All segments along the CRF are believed to be blind faults except for those within the Hoping segment. These two opposite reverse dominated dip-slip faults intersect near the surface as a result of the ongoing suturing process and rapid exhumation of the Central Range. An understanding of how active the faults are at greater depths is crucial for understanding the tectonic kinematics and future evolution of Taiwan.

The Chihshang segment along the LVF has been documented to be continuously creeping at the ground surface (e.g., Angelier et al., 2000; Lee et al., 2003). The interseismic fault coupling model using Persistent Scatterer SAR Interferometry (PS-InSAR), GPS, leveling, and creepmeter data illustrates that the 2003 M_L 6.4 Chengkung earthquake (e.g., Chang et al., 2009; Hsu et al., 2009) occurred in a zone on the Chihshang fault with a high coupling ratio (Thomas et al., 2014). Due to the poor resolution obtainable for depths greater than 10 km (reaching offshore), a definitive analysis of how and where fault creep at depth remains needed. The CRF on the other side of the valley has produced many uplifted lateritic fluvial terraces and is believed to be active to the south and inactive to the north (e.g., Shyu et al., 2006). The activity at greater depths, however, is unclear due to the scarcity of surface rupture evidence and the unavailability of geodetic data across it.

Seismological observations such as repeating earthquakes serve as powerful tools for studying the spatiotemporal distribution of aseismic slip behavior at depth. Repeating earthquake sequences (RES) are groups of earthquakes that have nearly identical waveforms, sizes, and locations. Given that magnitude and recurrence interval are sensitive to the loading conditions of a fault, RES can provide an independent measure of slip rate at depth (Beeler et al., 2001; Chen & Lapusta, 2009; Chen, Nadeau, & Rau, 2007; Chen, Yen, et al., 2007; Igarashi et al., 2003; Nadeau & Johnson, 1998; Sammis & Rice, 2001). Rau et al. (2007) and Chen et al. (2008, 2009) analyzed 55 RES (containing 215 events in total) from two separate segments along the LVF and CRF in eastern Taiwan. From 1991 to 2004, they established the variability of the deep slip rate and the different spatiotemporal behavior of repeating events in the Chihshang and Hualien regions. The number of RES within the period from 2000 to 2011 is 202 (containing 1,161 repeating events). This updated RES catalog allows us to further study the space and time-dependent fault behavior of the LVF and CRF at depth. In this study, we re-examine the methods of slip rate estimation for regional differences in creep behavior and explore how the RES responded to large earthquakes in their vicinity.

2. Repeating Earthquake Identification

RES have been used to detect fault creep and the locations where the creep and the locked areas of the faults meet (Bürgmann et al., 2000; Chen & Lapusta, 2009; Malservisi et al., 2005; McLaskey & Kilgore, 2013; Sammis & Rice, 2001). They are regarded as fault slip rate indicators (Nadeau & McEvilly, 1999; Nadeau & McEvitty, 2004; Uchida et al., 2003). The minimum threshold of the cross-correlation coefficient (CCC) has been widely used to identify RES (Igarashi et al., 2003; Nadeau & Johnson, 1998; Templeton et al., 2008; Uchida et al., 2003). In eastern Taiwan, the one-sided distribution of seismic stations with low signal-to-noise ratios (SNRs) makes CCC-based identification challenging, and so, in this study, we adopted the composite selection approach proposed by Chen et al. (2008), which considers both waveform similarity and differential S-P time (dS_mP) information. The thresholds in CCC and dS_mP however are refined by the consideration of frequency-dependent behavior for different magnitude.

This study examined data from 72,761 earthquakes of $M_L \geq 2$ from the Central Weather Bureau Seismic Network catalog during the study period of 1 January 2000 to the end of 2011 with a quality rating of C or better (data quality ratings range from A to D, where A is the best rating). The vertical component of the short-period seismograms with a 100-Hz sampling rate was first band-pass filtered to 2–8 Hz for

cross-correlation computation. Each seismogram was cut from 3 s before P arrival to 27 s afterward. Those events having seismogram pairs with CCC greater than 0.9 at more than three stations were selected. The data set was then generated for the final manual check by requiring a small dS_mP between events (≤0.02 s) in CCC ≥0.9 event pairs of each similar cluster. To ensure at least 50% overlap of source area for the repeating events, the normalized distance (i.e., the interevent distance divided by the sum of the rupture radii of two events) should be smaller than 0.4. The interevent distance (dL) is a function of dS_mP and wave velocity Vp and Vs as $dL = dS_mP \times \frac{VpVs}{Vp - Vs}$. The rupture radius ($r$) on the other hand is determined using $\sigma = \frac{7M_0}{16r^3}$, where the M_0 and σ represent seismic moment and static stress drop, respectively. By assuming 3-MPa stress drop, Vp = 4.0 km/s, and Vp/Vs = 1.78, we found that the $dS_mP \leq 0.02$ s serves as a reasonable threshold for $M_L \geq 2.5$ events but not for smaller events. For smaller events of $M_L < 2.5$, a stricter dS_mP threshold of 0.01 s is applied. Magnitude-dependent dS_mP constrained by 50% source overlap can be illustrated by Figure S1 in the supporting information. Using the above criteria, we identified 202 RES in eastern Taiwan that contain 1,161 repeating events with magnitudes ranging from 2.0 to 4.6. The RES denoted by the blue circles in Figure 1 are mainly located within the two boxes representing the Chihshang and Hualien areas.

Based on the lifetime (time span between the first and last event in a sequence), the RES can be classified into burst-type (lifetime < 3 years) and continuous type (lifetime ≥3 years). Burst-type sequences are primarily characterized by their very short recurrence interval, are likely to be associated with triggering or fluid-related processes (Duverger et al., 2018; Igarashi et al., 2003; Vidale & Shearer, 2006), and are excluded from the following calculation of the deep slip rate. By calculating the coefficient of variance (COV) of the recurrence interval (Tr), we further classified the continuous type of RES into quasiperiodic types (Q type: COV ≤ 0.3) and aperiodic types (A type: COV > 0.3) (Chen et al., 2008, 2009). Here the COV in Tr for each sequence is determined by

$$COV\ in\ Tr = \sqrt{\sum_{i=2}^{N}\left(Tr - Tr_{avg}\right)^2/(N-1) \times {Tr_{avg}}^2}, \quad (1)$$

where Tr and Tr_{avg} represent the individual and averaged recurrence intervals in a sequence, respectively, and N represents the total number of events in a sequence. The COV in seismic moment (Mo) can be also calculated similarly by

$$COV\ in\ Mo = \sqrt{\sum_{i=2}^{N}\left(Mo - Mo_{avg}\right)^2/(N-1)*{Mo_{avg}}^2}, \quad (2)$$

where Mo and Mo_{avg} represent the individual and averaged seismic moment in a sequence, respectively, and N represents the total number of events in a sequence. Figure 2 shows an example of the identical waveforms from the Q-type and A-type sequences. The A-type RES in both the Chihshang and Hualien areas have a similar magnitude range of 2.0 to 4.1 (Figure 3b), whereas the Q-type RES in the Hualien area have a greater magnitude (M_L 2.1–4.6) than those in the Chihshang area (M_L 2.1–3.3) (Figure 3a). For A-type RES, the COV in Tr and Mo tends to be slightly higher in the Hualien area than the Chihshang area (Figures 3d and 3f). The Q-type RES also have slightly higher moment variation in the Hualien area (Figure 3e). In summary, the RES in the Hualien area have a higher magnitude range and greater variation in both the recurrence interval and seismic moment. There is no clear spatial distinction for the Q-type and A-type sequences in the two areas (represented, respectively, by red and dark red circles in Figure 4). Among the A-type RES, there are sequences that show a clear relationship with a mainshock. They are further identified as (1) new type (N type)—the onset of the sequence occurred after the mainshock and (2) influenced type (I type)—at least one event occurred before the mainshock, and the recurrence interval was significantly shortened after the mainshock. The I-type and N-type RES are only found in the Chihshang area (on the creeping Chihshang fault), which were strongly influenced by the 2003 M_L 6.4 Chengkung mainshock.

3. Distribution of Repeating Earthquakes

As mention earlier, the RES are highly concentrated in eastern Taiwan, separated into the two areas of Chihshang and Hualien (represented by boxes in Figure 1b). In the Chihshang area, a total number of 73

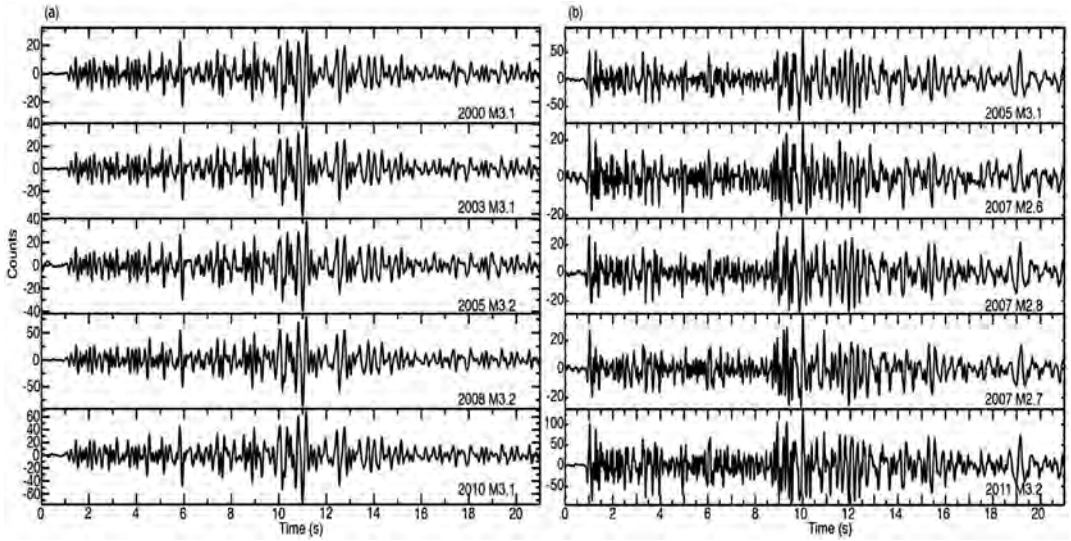

Figure 2. Vertical component of the waveform examples for (a) quasiperiodic (Q-type) RES with an average magnitude of M_L 3.2 and (b) aperiodic sequence (A-type) RES with an average magnitude of M_L 2.9. The waveforms were recorded at station SML and TWG for (a) and (b), respectively.

RES composed of 378 repeating events (M_L 2.1–4.1) occurred within the area between 121.1°E to 121.5°E and 22.8°N to 23.3°N. Their magnitude, location, and averaged recurrence interval information are listed in the supporting information as initial of CH. They coincide with the east-dipping Chihshang segment of the LVF (cross sections 2–4 in Figure 4). The focal depths of the RES mainly range from 7 to 25 km. Note that a small group of RES in cross section 1 is located underneath the valley and eastern flank of the Central Range. They likely belong to a separate structure and are not considered in the further calculation of the regional slip rate for the Chihshang fault.

To the north of 23.5°N, the RES occurred along a west-dipping CRF and are mostly concentrated at depths greater than 8 km (cross sections 5–9). This area spans most of Hualien county and is therefore referred to as the Hualien area. The RES in this area form two separate groups. One group is located underneath the Central Range (cross sections 5–7), and the other group is located inside the seismicity cluster that appears in cross section 8 and expands toward the north. This cloud-like seismic cluster denoted by a dashed circle in Figure 4 (cross sections 8–10) represents the contact of the Eurasian plate and Philippine Sea plate where the Eurasian plate straddles the colliding/subducting Philippine Sea plate (Wu et al., 2009). This is a complex transition zone from NW collision to northward subduction, corresponding to a west-dipping and north-dipping structure, respectively. In the map view, the two groups are separated by a valley, forming the eastern and western Hualien areas, hereafter referred to as HE and HW, respectively. The majority of the RES in the Hualien area are located in HW, and their depths are likely greater to the north (minimum depth of 8 km at cross section 5 and 15 km at cross section 8). The 114 RES found in the Hualien area are composed of 719 repeating events with magnitudes ranging from 2.0 to 4.6. Among them, there are only 27 RES found in HE, which consist of 137 repeating events with magnitudes ranging from 2.1 to 4.3, and they are mainly concentrated at depths of 7–15 km (RES in the dashed circles at cross sections 8–10 in Figure 4).

The magnitude, location, and averaged recurrence interval information for the sequences in the Hualien and Chihshang areas are listed in the supporting information (Table S1) as initial of HU and CH, respectively. The information for individual events is shown in Table S2.

4. Slip Estimate of Individual Repeating Sequences

Assuming repeating events in a RES rupture the same fault patch and have the same long-term slip rate on the whole fault plane, the deep slip rate can be obtained from the recurrence interval and the average of the seismic moment (Nadeau & McEvilly, 1999). Using M_L obtained from the Central

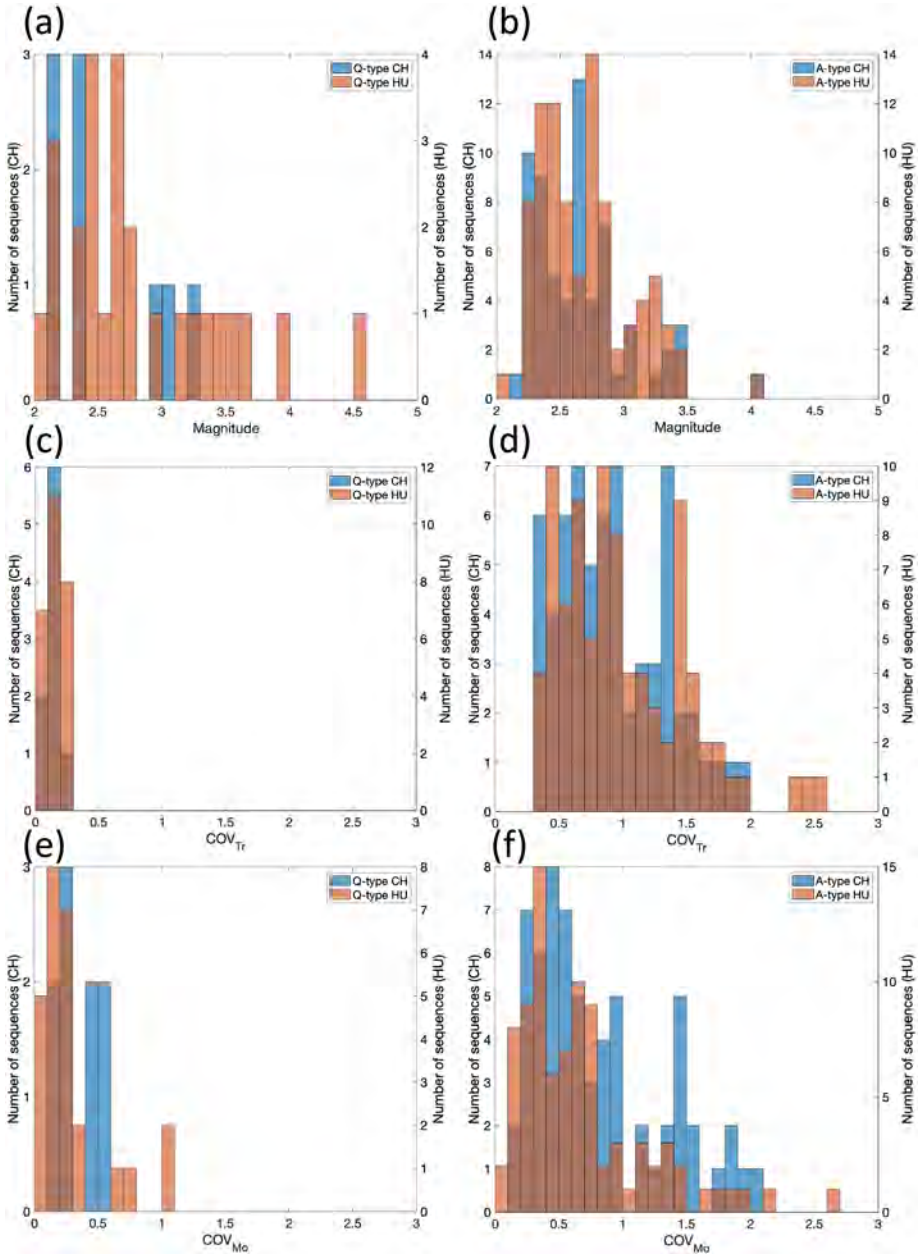

Figure 3. Number of RES for (a and b) event magnitude, (c and d) COV in recurrence interval (*Tr*), and (e and f) COV in seismic moment (*Mo*) for quasiperiodic (Q-type) and aperiodic (A-type) sequences in both the Chihshang and Hualien areas. The RES for the Chihshang and Hualien areas are indicated by blue and orange, respectively. The rightward vertical axes denote the number for the Hualien area, whereas the leftward vertical axes denote the number for the Chihshang area.

Weather Bureau earthquake catalog, we used the relationship below to determine M_W (Huang et al., 2000):

$$M_W = (0.91 \pm 0.03)M_L + (-0.07 \pm 0.15). \quad (3)$$

Here M_W is further converted to the seismic moment (in dyne-cm) using the equation below from Hanks and Kanamori (1979):

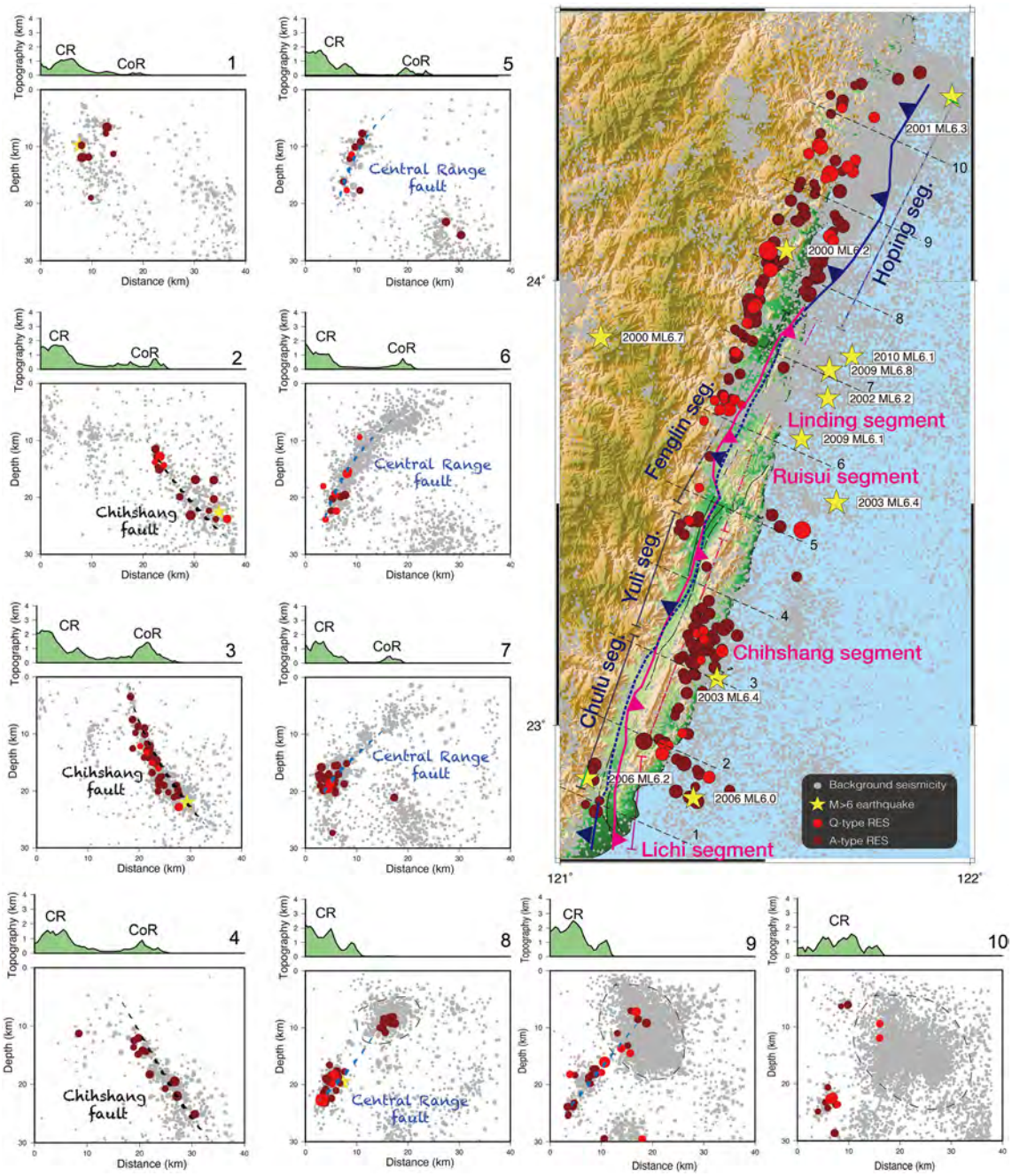

Figure 4. Cross sections of background seismicity (gray dots) and RES (red circles). The two RES strands in the Hualien area are associated with the Chihshang fault and the Central Range fault, as indicated by thick dashed lines. The seismic events encircled by thin dashed lines in cross sections 8 to 10 denote a cloud-like structure extending offshore. Yellow stars represent $M_L > 6$ earthquakes. Q-type and A-type sequences are denoted by red and dark red circles, respectively. CR stands for Central Range, and CoR stands for Coastal Range.

$$\log M_o = 1.5(M_W + 10.73). \quad (4)$$

The sum of the moment release from the repeating events in a sequence leads to $\sum M_0 = \mu A \sum D$ (Aki, 1966), where A and $\sum D$ represent the averaged rupture area and cumulative slip, respectively. Assuming the cumulative slip is a result of tectonic loading from the surroundings over one seismic cycle and can be represented

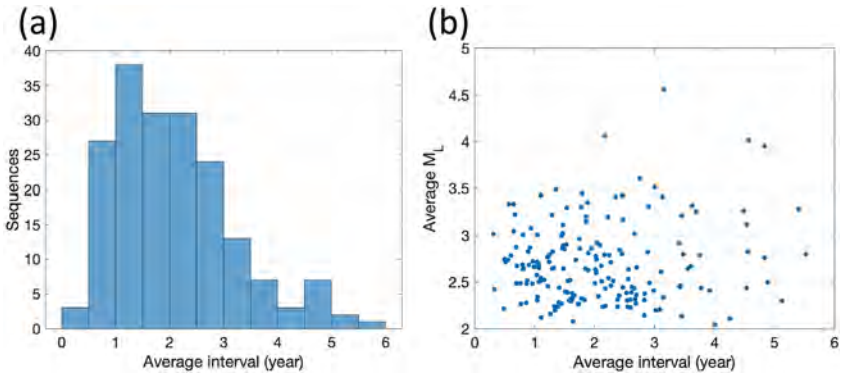

Figure 5. (a) Histogram of averaged recurrence intervals for each repeating earthquake sequence in the study area. (b) Plot of averaged magnitude versus recurrence interval.

by the GPS-derived interseismic slip rate $\dot{\tilde{d}}$, the cumulative moment release smoothed over the duration T_i can then be described as follows:

$$\dot{\widetilde{M_0}} = \frac{\sum M_0}{T_i} = \mu A \dot{\tilde{d}}, \tag{5}$$

where A represents the averaged rupture area, which can be obtained using known $\dot{\tilde{d}}$ and $\dot{\widetilde{M_0}}$. This then allows us to determine the slip for individual repeating events using the equation

$$d = \frac{M_0}{\mu A}. \tag{6}$$

The inferred d represents aseismic slip in the immediate surroundings of the RES.

In this study, the rupture area A and seismic moment release rate $\dot{\widetilde{M_0}}$ for each repeating sequence are first computed using equation 5, and slip for each event in the same sequence is inferred using equation 6. For individual sequence, the time history of slip reflects the slip rate in the surrounding creeping area, which is controlled by the recurrence interval (Tr) and magnitude of the events in a sequence. When the variation in recurrence interval and seismic moment grows, the stronger time dependency appears. In this case, a missing event in individual sequence could lead to considerable uncertainty in creep rate. As shown in Figure 5a, during the study period of 12 years, the averaged Tr for each sequence ranges from 0.318 to 5.527 years. Most of sequences reveal the averaged Tr of 1–3 years, while few sequences are characterized by $Tr \geq 4$ (7% of total repeating sequences). The longer Tr is not necessarily corresponding to greater magnitude (Figure 5b). Smaller magnitude sequences could end up showing longer Tr, which is likely a result of missing events in a sequence. The sequences with abnormal Tr, although exist, only play a minor role in our regional slip rate measurement (will be elaborated in the next session) due to its small population comparing with the total number of sequences (i.e., 13 out of 187 for $Tr \geq 4$ and 33 out of 187 for $Tr \geq 3$).

The recurrence interval is believed to be strongly controlled by the size of earthquake. The study of repeating earthquakes in Parkfield reveals a scaling relation between Tr and Mo that requires higher stress drop or the involvement of aseismic slip (Nadeau & Johnson, 1998). Later, this scaling is found to be remarkably consistent among different regions after accounting for differences in the geodetically derived slip rate (Chen, Nadeau, & Rau, 2007; Chen, Yen, et al., 2007; Dominguez et al., 2016; Yu, 2013). Therefore, the Tr-Mo scaling is regarded as a useful tool to constrain the averaged slip rate, which may provide the first hand difference of creep rate between the Chihshang and Hualien areas.

To check if the close-by RES reveal similar creep rate $\dot{\tilde{d}}_{RES}$ (cumulative slip over time, $\sum d/T_i$), we performed a slip rate ratio for the close-by RES pairs. Each of the 202 repeating sequences in both the Chihshang and Hualien areas is paired with the closest sequence, to obtain the intersequence distance and the ratio of creep rate between two sequences. As shown in Figure S2, the median value for data in each 0.1-km bin is confined

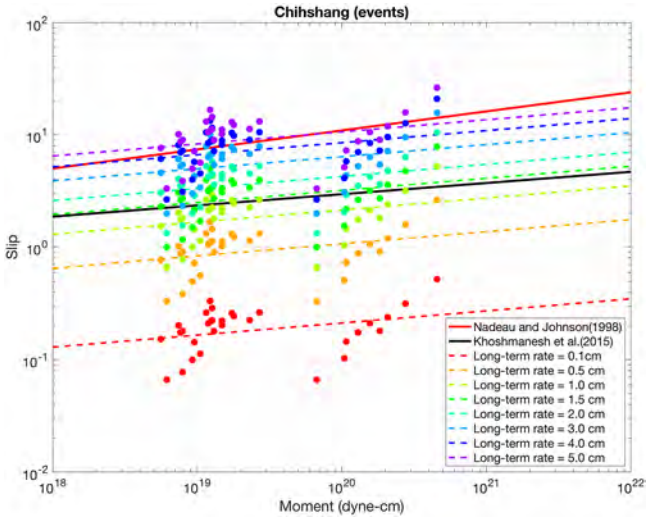

Figure 6. The slip inferred from the quasiperiodic RES' recurrence interval, seismic moment rate, and the assumed long-term slip rate of the Chihshang area (colored circles and dashed lines) and the comparison with the empirical relationship inferred from repeating events in Parkfield, California (solid red and black lines). Note that in this sensitivity test, only the quasiperiodic sequences (COV $\leq$ 0.3) are considered.

near 1 within a distance of 2 km. This suggests that the creep rate for neighboring sequences is highly similar, consistent with the hypothesis of RES, which are driven by the creep in the surrounding.

5. Sensitivity of Long-Term Slip Rate to Slip Estimates of RES

The GPS-derived interseismic slip rate $\dot{\bar{d}}$ in equation 5 may play an important role in creep rate estimate $\dot{\bar{d}}_{RES}$. To understand how much the assumed $\dot{\bar{d}}$ controls $\dot{\bar{d}}_{RES}$, we next conduct a sensitivity test and compare with the previously proposed $d_i - Mo$ empirical relationships. In the hanging wall of the Chihshang fault, the age data for river terraces reveal a long-term uplift rate of 2.2–2.4 cm/year, which is generally consistent with the short-term leveling measurements (Mu et al., 2011). Slip rate inversion using the 1999–2004 creepmeter data (Lee et al., 2006) reveals an interseismic slip rate of 2.6 and 3.8 cm/year above and below the depth of 87 m, respectively (Chang et al., 2009). A joint inversion using widely distributed InSAR, GPS, leveling, and creepmeter data from 1992 to 2010 inferred the pre-2004 interseismic slip rate as 4.4 cm/year at the depth of 0–15 km, whereas the result is less reliable at greater depth (below 15 km) due to the poor resolution of inversions (Thomas et al., 2014, 2017). The interseismic slip model by Thomas et al. (2014) reveals strong spatial variation of interseismic slip rate along-strike and along-dip directions due to a combination of heterogeneous frictional properties and stresses. Given that the majority of repeating earthquakes are located deeper than 7 km, the 4.4-cm/year rate of Thomas et al. (2014, 2017) at the depth above 15 km was adopted. Using the geodetically inferred slip rate of 4.4 cm/year, we obtained a scaling relationship between the slip estimate and seismic moment (*d-Mo*):

$$\log d_i = \alpha + \beta \, log M_0, \tag{7}$$

where α and β have been determined to be −1.21 and 0.11, respectively. Using the 25 M_L 2.1–4.6 RES and 12 GPS stations near the CRF, Rau et al. (2007) obtained an interseismic fault slip rate of 4.7 cm/year at depths greater than 10 km. For CRF, we thus adopted the 4.7 cm/year to infer the α and β as −1.96 and 0.14, respectively.

We performed a sensitivity test of α and β for long-term slip rates ranging from 0.5 to 5.0 cm/year. In Figure 6, slip estimates from different assumption of long-term slip rates are shown by colorful dots. The linear trend formed here is a proxy of previously mentioned *Tr-Mo* relationship, where the slip for a RES should be proportional to *Mo* due to the ideally, constant rupture radius. In the observation, the small variation in rupture radius exists, leading to the scattering in Figure 6. Various assumption of long-term slip rates results in a constant β (0.11) but a variable α ranging from −2.82 to −1.14.

Note that the same scaling relationship was previously investigated from the RES along San Andreas fault (SAF). Nadeau and Johnson (1998) used 55 sequences in Parkfield to obtain an α and β of -2.36 ± 0.16 and 0.17 ± 0.009, respectively. This was later confirmed by repeating earthquake data from Japan and Taiwan (Chen et al., 2008; Chen, Nadeau, & Rau, 2007; Chen, Yen, et al., 2007; Uchida et al., 2003). Using an InSAR-derived interseismic slip model, Khoshmanesh et al. (2015) further modified these variables to $\alpha = -1.53 \pm 0.37$ and $\beta = 0.10 \pm 0.02$, which provides a better fit with the time-dependent creep model across the central SAF. The *d-Mo* relation established for the central SAF is superimposed onto Figure 6 (the solid lines), in order to compare with the slip estimates from the repeating events on the Chihshang fault (colorful dots). Note that the data from the Chihshang fault are obtained using the original forms of equations 5 and 6. The empirical function from Nadeau and Johnson (1998) appears to serve as the upper bound (the red solid line in Figure 6). The regression lines located within the two scaling lines determined by Khoshmanesh et al. (2015) and Nadeau and Johnson (1998) correspond to the long-term slip rate of 1.5–5.0 cm/year. The same practice for the Hualien area yields a similar result, as shown in Figure 7. Varying the long-term slip

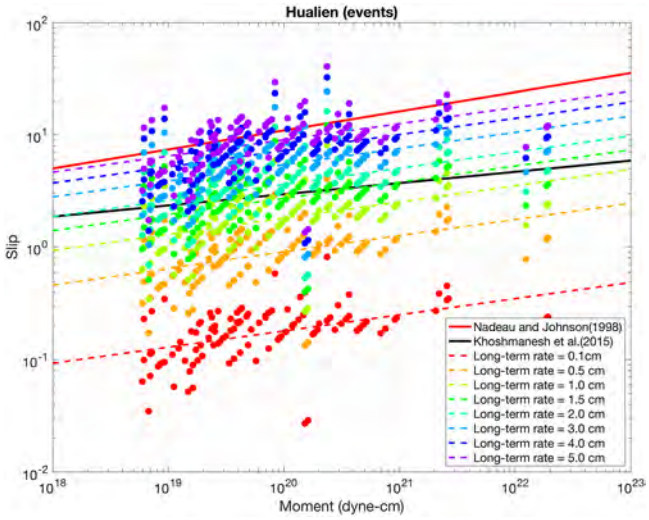

Figure 7. The slip inferred from the RES' recurrence interval, seismic moment rate, and the assumed long-term slip rate of the Hualien area (colored circles and dashed lines) and the comparison with the empirical relationship inferred from repeating events in Parkfield, California (solid red and black lines). Note that in this sensitivity test, only the quasiperiodic sequences (COV $\leq$ 0.3) are considered.

rate changes α (−2.62 to −0.92) but not β (0.14). The general population of slip estimates with various long-term slip rates is similar to the one for the Chihshang area. The regression lines (dashed lines in Figure 7) located within the two solid lines determined by Khoshmanesh et al. (2015) and Nadeau and Johnson (1998) correspond to the long-term slip rates of 1.5–5.0 cm/year. This comparison is an evidence of the regional dependency of the scaling law between slip and magnitude. Figures 6 and 7 also imply that the determination of slip for individual repeating event is sensitive to long-term slip rate assumed on the fault. In the next session, we will further examine how the regional slip rate changes with different scaling laws.

6. Determination of Regional Slip Rates

The creepmeter data provide a constraint for slip rates calculated from RES. Note that the east-dipping main fault is found to develop into a diffused zone composed of several small faults near the surface (Lee et al., 2003, 2006; Mu et al., 2011). The creepmeters were deployed to record the horizontal shortening across a 120-m-wide deformation zone that represents most of slip on the primary fault plane at the surface level. In this study, we used the data from three rod-type creepmeters installed on three branches of the Chihshang fault that accommodate most of the deformation in a narrow zone (Lee et al., 2003). To be comparable with RES data, we updated the study period from 1998 to 2009 (Lee et al., 2003; Mu et al., 2011) to 2000–2011 with a sampling interval of 1 day. We combined time series from three creepmeters to present the shortening rate across a wide deformation zone.

To obtain the average slip rate history from RES, we used different slip versus moment scaling laws determined from (1) the RES data in the Chihshang area assuming 4.4-cm/year long-term slip rate, (2) the RES data in Parkfield and Stone Canyon by Nadeau and Johnson (1998), assuming 2.3-cm/year long-term slip rate, and (3) the same RES data in Nadeau and Johnson (1998) but with the spatially heterogeneous slip rate by Khoshmanesh et al. (2015). In Figure 8, the resulting slip rates from the different scaling laws (listed above) are compared with the slip history from the creepmeter data. The creepmeter provides a direct measurement for the temporal evolution of fault creep on the surface. Given that the shortening rate from creepmeters is likely equal to or less than the slip along the fault at greater depths, it can thus serve as the lower bound of interseismic slip rate in the creeping segment. Note that for Figure 8, the cumulative slip was divided by the total number of sequences in the area to obtain the normalized cumulative slip. The absolute value of the regional slip rate was found to be sensitive to the choice of *d-Mo* scaling law. Among the

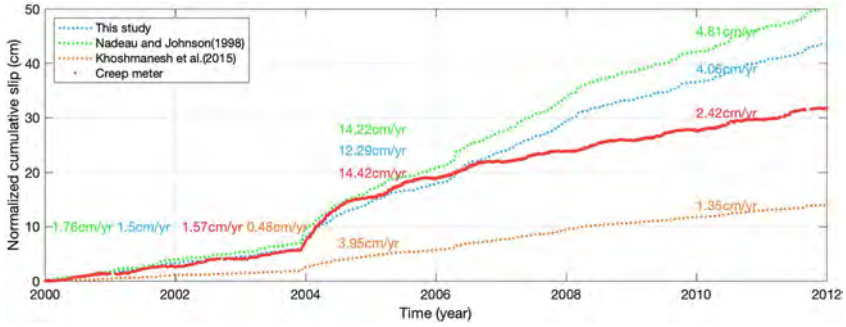

Figure 8. Cumulative slip as a function of time for the Chihshang area. The result of this study represents the slip obtained by equation 7, with α and β determined to be −1.21 and 0.11, respectively. The slip determined from the *Mo*-slip scaling relation by Nadeau and Johnson (1998) requires an α and β of −2.36 and 0.17, while that of Khoshmanesh et al. (2015) requires α and β to be −1.53 and 0.10, respectively. Note that in this regional slip rate estimate, all sequences (both quasiperiodic and aperiodic) are considered.

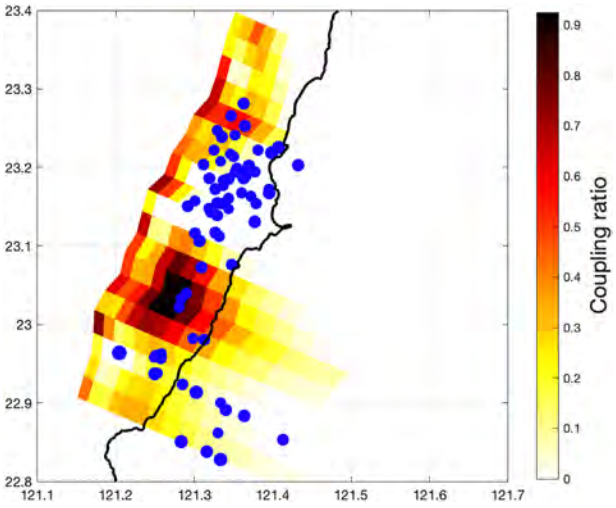

Figure 9. Coupling ratio on the Chihshang fault by Thomas et al. (2014) and the distribution of RES found in this study. Blue circles represent RES on the same fault. Background color on the fault indicates a different coupling ratio.

different measurements, the result from the *d-Mo* scaling law by Nadeau and Johnson (1998) serves as an upper bound for the regional slip rate (green dashed lines in Figure 8), whereas the result by Khoshmanesh et al. (2015) exhibits much lower slip rate (orange dashed line). Before the 2003 M_L 6.4 earthquake, the magnitude of slip rate derived from this study (1.5 cm/year) is similar to those inferred from creepmeter (1.6 cm/year) and from the *d-Mo* relationship by Nadeau and Johnson (1998) (1.8 cm/year). Around 6 months following the M_L 6.4 Chengkung earthquake, the slip rates from the above measurements are increased to 12.3, 14.4, and 14.2 cm/year, respectively, about 8–10 times greater than the preseismic level. After the year of 2004.5, the slip rate inferred by this study drops to 4.1 cm/year and remains stable until the end of 2011. The creepmeter reveals lower slip rate (2.4 cm/year) comparing with the value inferred from this study (4.1 cm/year), while the result from *d-Mo* scaling law by Nadeau and Johnson (1998) shows higher value of 4.8 cm/year. This trend (slopes of green dashed line > blue dashed line > red line) after 2003.5 is the same with that observed during the preseismic period (2000 to December 2003), indicating that the interseismic creep rate at depth inferred from RES is generally higher than the surface creep. We also found that the location of the repeating events coincides with the low coupling ratio inferred by Thomas et al. (2014) (Figure 9). More than 64% repeating events are located in the areas showing coupling rate lower than 0.1. This may explain why deep creep rate tends to be bigger than surface creep rate. The *d-Mo* scaling relation derived in this way (assuming 4.4-cm/year long-term slip rate) is thus considered a valid measure for the regional slip rate.

For the Hualien area where surface creep data were not available across the fault, we used the recurrence behavior as a constraint. As established by Chen, Nadeau, and Rau (2007) and Chen, Yen, et al. (2007), *Tr-Mo* scaling is mainly controlled by the difference in regional tectonic loading rates. When the logarithm of the averaged recurrence interval is plotted against the logarithm of the average seismic moment from Figure 10a, the majority of the RES from the Chihshang and Hualien areas overlap (open symbols). Their recurrence intervals are 2–3 times shorter than those expected from the RES in Parkfield of the SAF (red diamond). When we normalized the recurrence intervals of these two areas by the ratio of the loading rate (4.4 cm/year for Chihshang and 4.7 cm/year for Hualien) to the rate used for the Parkfield repeating earthquake data (2.3 cm/year), they fit the same regression line (Figure 10b). This indicates that the long-term slip rate of the Hualien area is similar to or slightly higher than the one assumed for the Chihshang area. This *Mo-Tr* scaling provides another constraint for the difference in tectonic loading, which is not conflict with consistent with the loading rates of 4.7 cm/year for the Hualien area from Rau et al. (2007) and 4.4 cm/year for the Chihshang area (Thomas et al., 2014).

7. Temporal Distribution of the Regional Slip Rates

7.1. Cumulative Deep Slip Rate: Regional Difference

The resulting regional creep rates in the Chihshang and Hualien areas are shown in Figure 11. The black line in Figure 11 is the same with the blue dashed line in Figure 8. Prior to the mainshocks (from 2000 to December of 2003), the deep creep rate is inferred as 1.5 cm/year. A sudden acceleration in deep slip rate occurred at the end of 2003 as a result of the 2003 M_L 6.4 Chengkung earthquake. From December 2003 to March 2004, the deep creep rate increased to an average value of 12.3 cm/year and then dropped to 4.1 cm/year until the end of 2011. There exists a significant increase in the postseismic deep slip rate comparing with the preseismic level. The surface deformation from the creepmeter, however, shows only a minor increase in the creep rate from 1.5–1.8 cm/year up to 2.0 cm/year since March 2004 (Mu et al., 2011). This suggests that since mid-2004, the postseismic effect has lasted for a much longer time at greater depths where the RES occurred (deeper than 7 km), while a slip rate deficit existed at depths less than 7 km. In space, the RES in the Chihshang area can be separated into two segments by visual inspection. As shown in Figure 11a, the repeating events tend to cluster more closely in the northern segment (blue circles), which has been previously recognized as creep by the occupation of all repeaters in the 1991–2003 RES catalog (Chen

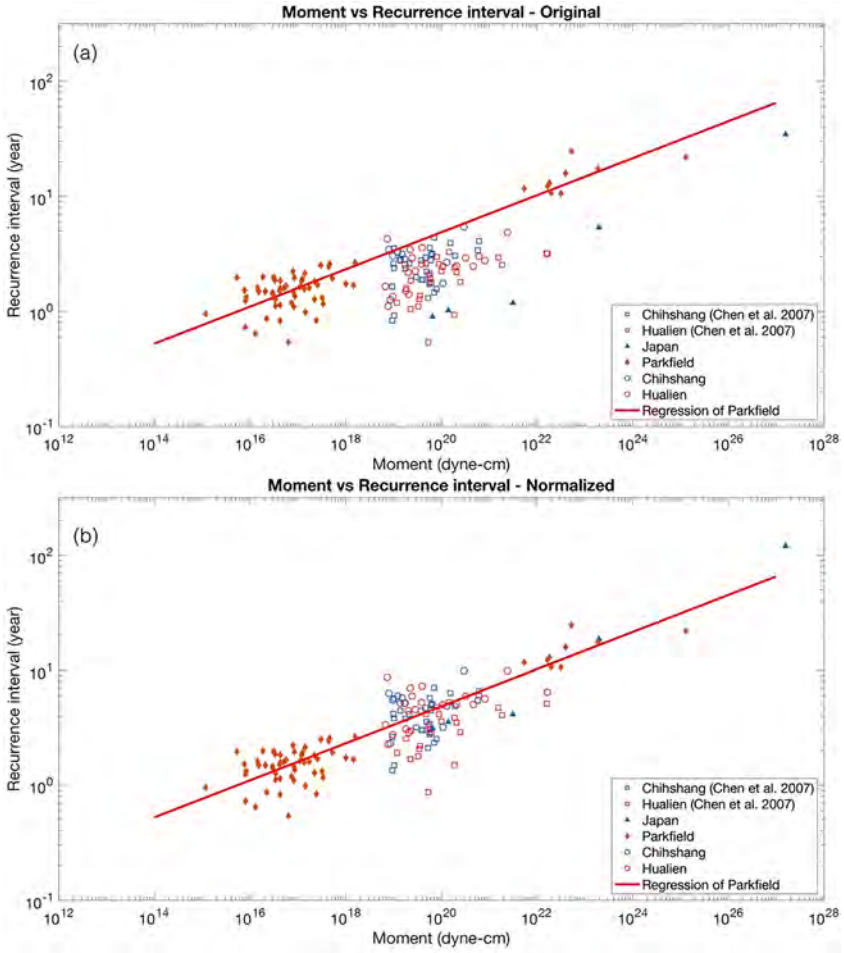

Figure 10. Recurrence interval as a function of seismic moment for the quasiperiodic RES from Parkfield, Japan, and Taiwan. Each symbol represents the average value for each sequence. The 10 and 21 RES from the Chihshang and Hualien areas are shown by blue and red open circles, respectively. Data for Parkfield, Japan, and Taiwan as indicated by diamonds, triangles, and open squares, respectively, are from Chen, Nadeau, and Rau (2007) and Chen, Yen, et al. (2007).

et al., 2008). To the south where the fault trace is not mapped (absence of black line in Figure 11a), the RES tend to be more widely distributed (the red circles in Figure 11a). In temporal behavior, the two separate groups have a similar pattern (the red and blue lines in Figure 11b), especially with regard to the acceleration effect from the M_L 6.4 Chengkung event. The southern group, however, experienced another elevated slip at the time of the two 2006 M_L 6.0 earthquakes in their vicinity. The different responses to the 2006 events may indicate distinct fault behavior for the north and south segments of the Chihshang fault.

The resulting creep rate in the Hualien area is shown in Figures 11c and 11d. As suggested in the cross sections in Figure 4, the repeating events can be grouped into two segments: The western group is located below the eastern flank of the Central Range at depths greater than 15 km, and the eastern group is distributed at shallower depths, likely corresponding to an offshore extension of the LVF. There exists a strong difference in the temporal distribution of creep between these two groups. As shown in Figure 11d, the western group (blue line) has a high slip rate of 4.3 cm/year that remains stable with time, whereas a much slower slip rate of 3.5 cm/year was found for the eastern group (red line). The distinct slip behavior is consistent with the separated clusters in cross sections 7–9 of Figure 4. Separated only by a distance of 3–6 km, the CRF to the west is characterized by a much faster creep rate than the LVF to the east. In the eastern Hualien area, the sudden acceleration of the creep rate was found to occur in mid-2005, which is a result of a swarm-like sequence of nine events that all occurred on 30 April 2005.

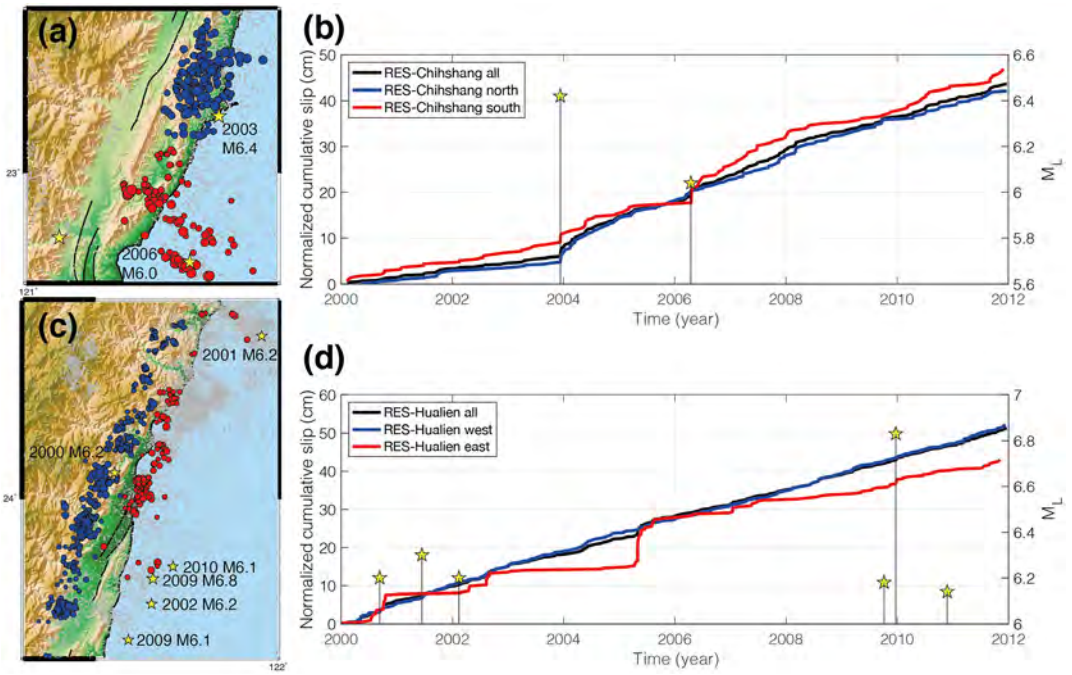

Figure 11. (a and c) The distribution of all repeating events in the Chihshang and Hualien area. Blue and red circles represent two different groups of repeating events that are spatially separated. The yellow stars indicate $M_L \geq 6$ earthquakes. (b and d) The cumulative slip as a function of time as inferred from the repeating events in the Chihshang and Hualien areas. Measurements from RES located in different subareas are indicated by blue and red lines, corresponding to the blue and red circles in (a) and (c). The black curve is derived from the repeating events in the whole area. The stars indicate the time and magnitude of $M_L \geq 6$ earthquakes.

7.2. Short-Term Slip Rates: Periodic Pulsing

A short-term slip rate can then be obtained by dividing the regional cumulative slip rate (in Figure 11) by a short time window. This is done by obtaining a median value using six different calculation windows (10, 30, 50, 100, 180, and 360 days) for 1-day time increment. That means that in each day, we determine the change of slip from 1 day before and 1 day after. The calculation window is used to average out the daily variation. Taking 10-day window, for example, we obtained the average from 10-day estimates prior to the target day. The median value (the red line in Figure 12a) reveals that the peaks with smaller slip rates (<1 cm/day) tend to be spiky with ~3 cycles per year, whereas the main peaks (≥1.5 cm/day) occurred in early 2004, early 2005, mid-2006, early 2008, late 2009, mid-2010, and late 2011 showing a semiannual recurrence. To ensure the determination of short-term rate is meaningful, the selection of calculation window should be longer than the length of data gap, which is the maximum interevent times of 115 days. We therefore selected a moving window of 180 days that is shorter than the interval between the main peaks (~1 year) and longer than the interval between the minor peaks (~108 days) and longest interevent time (115 days). The magnitude of slip rate is highly controlled by the number of events, as shown in Figure 12b. In a given calculation window, the near-zero slip rate can be produced because of no data. The longer calculation window produces bigger time shift of an actual signal. Applying cross-correlation function to check the maximum time lag produced by the 180 days window, we found that the time lag is less than 100 days. This implies that temporal resolution of our short-term slip rate variation is ~100 days. To ensure the comparability, in the following analysis we applied the same moving window scheme on different observations.

Using the 180-day moving window, the resulting short-term slip rate histories for the Chihshang and Hualien areas are shown in Figure 13. Both areas reveal regularly recurring slip rate pulses on a semiannual cycle. In the Chihshang area, the slip rate history shows a quasiperiodic pattern with a clear acceleration following the M_L 6.4 Chengkung earthquake on 10 December 2003. When the fast Fourier transform was applied to the time series of Figure 13a, the dominant frequency was found to decrease after the mainshock from ~1.1 years (the blue line in Figures 13b and 13c) to ~0.5 year (the red line in Figure 13b). The large

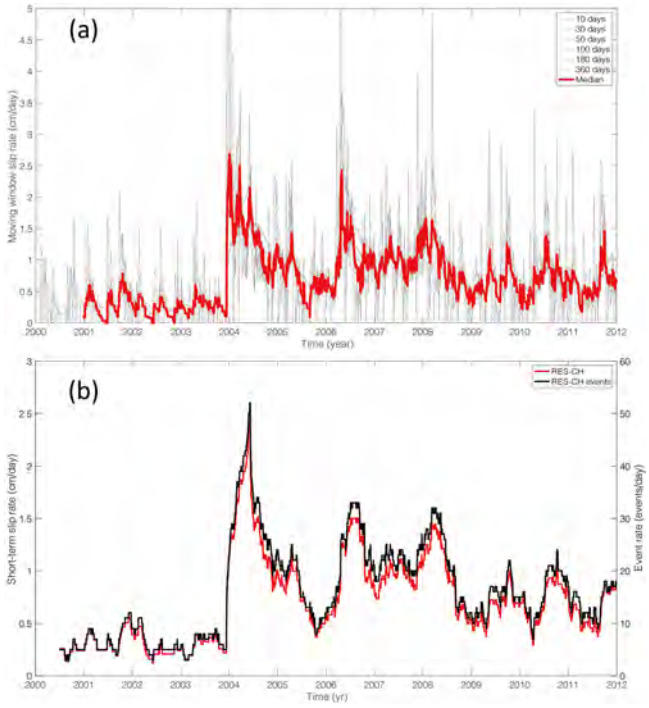

Figure 12. (a) Short-term slip rate versus time using different moving windows lengths of 10, 30, 50, 100, 180, and 360 days (gray lines) with 1-day time increments for the Chihshang area. The median value of the calculations from different window lengths is denoted by the red line. (b) Short-term slip rate and events rate versus time using 180-day window for moving window calculation. The red and black lines indicate slip and event rate separately.

variation in the peak amplitude of the spectrum is associated with the number of repeating earthquakes, evidenced by the fact that the 49 and 329 repeating events occurred during the premainshock and postmainshock periods, respectively.

The pattern of the short-term slip rate in the Hualien area, on the other hand, shows a regular pulsing of creep rate with an ~1-year interval over the study period (see the two peaks near 1 year in Figure 13e). The highest peak in the temporal variation of the creep rate in Figure 13d corresponds to the same acceleration shown in Figure 11d, which is a result of the swarm-like sequence that intensely occurred in 2005. This periodic pulsing pattern is similar to that seen in the Chihshang area during the premainshock period. The possible mechanism for this semiannual variation in deep creep rate will be addressed in section 9.

8. Spatiotemporal Distribution of the Regional Slip Rates

The spatial variation in the short-term slip behavior is well illustrated in Figure 14, where the slip rates are plotted at 0.01° increments along the latitude and 1-day time increments. An examination of the Chihshang area reveals relatively complex behavior, as the timing of the higher creep rate pulses (vertical warm color bars in Figure 14a) not entirely consistent across the area from north to south. The discontinuity of higher creep rate pulses in Figure 14a indicates a possible boundary at 23.0°N that demarcates distinct slip behavior. This boundary coincides with the beginning of the eastern-dipping fault zone in cross section 2 of Figure 4 (the Chihshang fault). The slip rates in the northern segment (north of 23.0°N) show a regular acceleration every 1–2 years, whereas the southern segment (south of 23.0°N) shows a slightly longer acceleration interval. The cumulative effect of the creep pulsing from the two different segments leads to a semiannual variation (the black line at the bottom of Figure 14a). The northern segment is strongly influenced by the 2003 M_L 6.4 Chengkung earthquake, whereas the southern segment is more influenced by the 2006 M_L 6.0 Taitung earthquake located offshore.

Unlike the complex creep rate pulses seen in the Chihshang area, the slip rates in the Hualien area appear to be quasiperiodic over the 12-year observation period. Such periodicity is concentrated between 23.85°N and 24.15°N showing no direct relationship with the occurrence of nearby large earthquakes (the white stars in Figure 14b). The periodic pulses represented by the warm color areas in Figure 14b coincide with the variation in the slip rate history (the black line at the bottom, the same as in Figure 13b), indicating that the repeating events located in the middle of the area are responsible for the dominant periodic features. Comparing the timing of the creep rate pulses in the Chihshang and Hualien areas, the semiannual pulses do not appear to be temporally linked. This suggests that the factor controlling the periodicity of the extensive aseismic slip may not be common for both faults.

9. Discussion

9.1. The Stress Drop Obtained From RES

Assuming a circular rupture, the static stress drop can be inferred using the equation below (Kanamori & Anderson, 1975):

$$\Delta\sigma = \frac{7\pi}{16}\mu\frac{d}{r}, \tag{8}$$

where μ is the shear modulus, d is the slip estimate, and r is the rupture radius. Here we use the *d-Mo* relationship inferred using the RES data in the Chihshang area ($\log d_i = -1.21+0.11 \log M_0$) to infer d. The

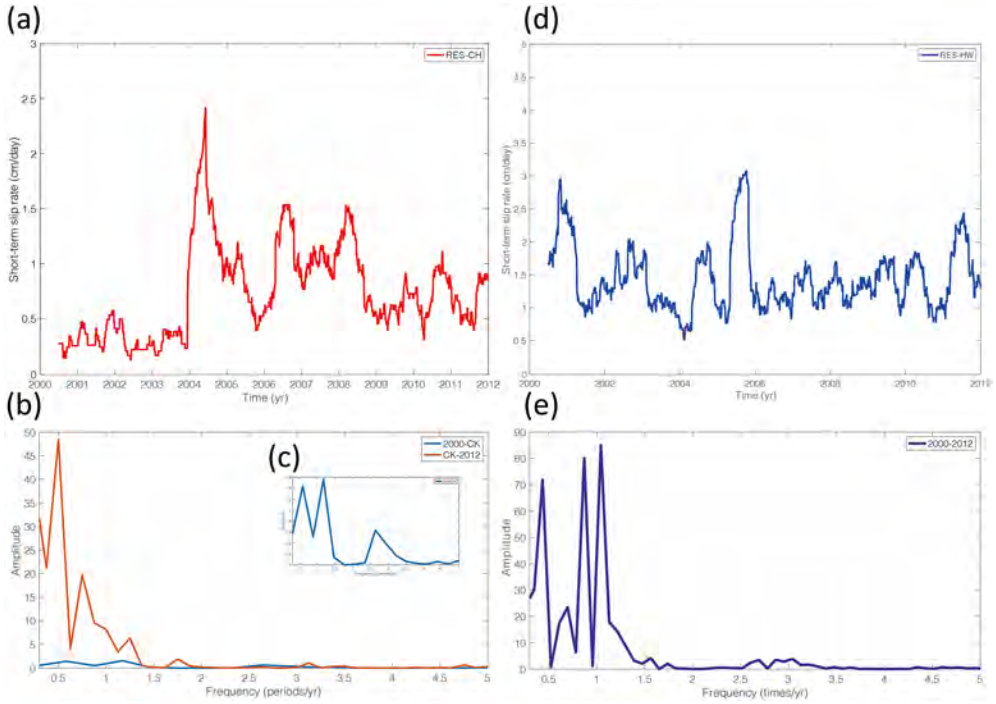

Figure 13. (a) Temporal variation of the short-term slip rate in the Chihshang area. (b) Short-term slip rate spectra for the premainshock (blue line) and postmainshock (blue and red lines) periods. (c) Detail view of (b) showing the main frequency of the pre–Chengkung period. (d and e) Temporal variation of the short-term slip rate and the corresponding spectra in the Hualien area. C. K. denotes the M_L 6.4 Chengkung event in 2003.

rupture radii ($R_d^{\sim}$) are derived from seismic moment rate and assumed geodetical long-term slip rate in equation 5. The stress drop for all repeating sequences (M_L 2.0–4.6) against seismic moment is shown in Figure 15, resulting in an empirical relationship of $\log(\Delta\sigma) = 14.2 - 0.56\log(Mo)$. The magnitude range of repeating sequences here compensates the data gap in Nadeau and Johnson (1998). There exists a clear dependency of stress drop on seismic moment, similar to what observed in central SAF. Chen et al. (2016) inverted the stress drop based on empirical Green's function for two M4 repeating sequences in eastern Taiwan. They obtained peak stress drop of 52.9–155.1 MPa (light gray box in Figure 15) with an averaged stress drop of 6.7–19.1 MPa (dark gray box in Figure 15). The peak stress drop is close to the regression line from RES data, while the averaged stress drop is located below. This indicates that the peak stress drop inferred using equation 5 is close to the finite source result. Such observation was also seen in M2 RES at Parkfield, indicating that the strong stress heterogeneity may be generally true over a range of magnitude from M2 in Dreger et al. (2007) to M4 in Chen et al. (2016).

The rupture radius used to constrain the colocation of earthquakes in this study is inferred by the equation below:

$$R_{\Delta\sigma} = \frac{7\pi}{16}\frac{M_0}{\Delta\sigma}. \tag{9}$$

If comparing radius determined using equations 8 and 9 by showing the ratio ($R_{\Delta\sigma}/R_d^{\sim}$), $R_{\Delta\sigma}$ is found to be 1–10 times larger than $R_d^{\sim}$. It suggests that the real rupture dimension allowing seismic slip is smaller than expected. To ensure the at least 50% overlap of source area, a more severe threshold in dS_mP is needed. The refined $dS_mP \leq 0.01$-s threshold in this study however may fail to act as constraint for the colocation of $M_L < 2.5$ events. The dS_mP threshold is sensitive to (1) the magnitude of target events and (2) the measurement/assumption of stress drop. Given the limitation in timing accuracy of the seismic data (Chen et al., 2008), we applied dS_mP thresholds with the assumption of 3-MPa stress drop. The better

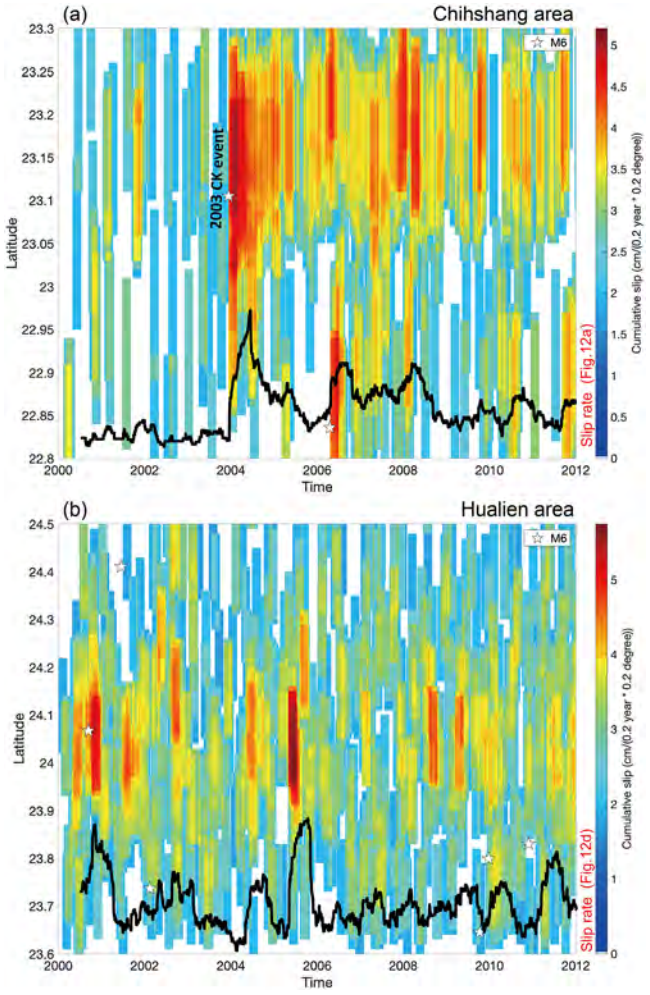

Figure 14. S-N profile of creep rate as a function of time for (a) the Hualien area and (b) the Chihshang area. The slip rate was determined using a 0.2 year by 0.2° window with 1-day and 0.01° increments. The repeating events used for the slip rate calculation are indicated by the blue and red circles in Figure 11. White stars indicate earthquakes with a magnitude greater than 6. The thick black line corresponds to the regional slip rate histories in Figures 13a and 13d.

threshold by considering higher stress drop can be obtained using other seismic network with higher SNR, less timing inconsistencies, and higher rate of sampling in the future.

9.2. Toward the Better Understanding of the Creeping Faults in Eastern Taiwan

The Chihshang segment on the LVF is an exceptional reverse fault on the world stage of continental creeping faults (Chen & Bürgmann, 2017; Harris, 2017). Recognized as a listric, thrust fault that has a geometrical steepening at shallower depth (<15 km) (Hu et al., 2007; Lee et al., 2006), the Chihshang fault is characterized by a velocity discontinuity of ~3 cm/year across the fault on the surface, causing obvious offsets in houses, roads, retaining walls, and pipes due to the cumulative slip over the decades (Angelier et al., 1997; Lee et al., 2000, 2001). At greater depths, contrasting fault slip behavior from north to south along the Chihshang fault was first deduced from the repeating earthquakes from 1991 to 2003 that occurred at a depth range of 7 to 23 km (Chen et al., 2008, 2009). The northern half of the Chihshang fault is creeping, and the southern half is partially locked, having a higher earthquake potential. Using four times as many repeating sequences as the catalog from Chen et al. (2008), the boundary for distinct creep behavior in the Chihshang segment was located at 23.0°N (Figure 14). North of the 23.0°N, the Chihshang fault is mainly creeping, with RES concentrated in a 20 × 20-km area having an averaged creep rate of 1.5 cm/year before the M_L 6.4 mainshock in December of 2003. This is also the area where the most quasiperiodic RES are located. South of the 23.0°N where Chen et al. (2008) inferred was a locked zone of the Chihshang fault, is corresponding to the coseismic slip zone of the 2003 M_L 6.4 event, and was found to be surrounded by sparsely distributed RES with a creep rate of ~2 cm/year before the mainshock (red line in Figure 11b). The higher slip rates found in the southern segment, therefore, could be simply a result of the spatially distributed creep rate from aperiodic RES. After the 2003 M_L 6.4 event, the afterslip dominated the regional creep behavior. The high slip rate was found to penetrate into the southern segment (to 22.85°N in Figure 14a), leading to similar range of creep rates (4.5–4.6 cm/year) from 2004 to 2006. The 2006 M6 event altered the slip history in the southern segment, leading to the return of the distinct slip behavior across 23.0°N.

Unlike the LVF, the activity of the CRF is less known. From 23.5°N to 23.9°N, there exists the different degree of subsidence between both sides of the Longitudinal Valley (Ching et al., 2011; Huang et al., 2010; Johnson et al., 2005), indicating the influence of subduction. However, no surface rupture of the CRF has been mapped (Biq, 1965). The geomorphic evidence of rising fluvial terraces indicates a maximum slip rate of 1.3 cm/year in the central CRF (Shyu et al., 2006). This plate Quaternate slip rate calculated at the Wuhe Tableland is near the epicenter of the 2013 M_L 6.4 Ruisui earthquake. The aftershocks and coseismic slip of this 2013 event were found to terminate at 23.7°N (Chuang et al., 2014), coinciding with the initiation of the RES cluster in the Hualien area. During the 2013 Ruisui earthquake, the coseismic slip mainly occurred at depths between 5 and 15 km, and the aftershocks were widely distributed from near surface to a depth of 25 km. To the north of the 2013 source area, the CRF is likely to change from a locked segment to an area of free creep at depths greater than 15–25 km (cross sections 6–9 in Figure 4). From 23.7°N to 24.4°N, the linear strand of RES is found to extend more than 80 km long. This deep creeping segment follows a different path from the northmost segment of the CRF (Hoping segment) defined by Chen et al. (2018) (Figure 1). Given that the CRF represents the geomorphological signature of the rapid growth and exhumation of the Central Range, the current study provides a seismological constraint on the nature of the northmost CRF:

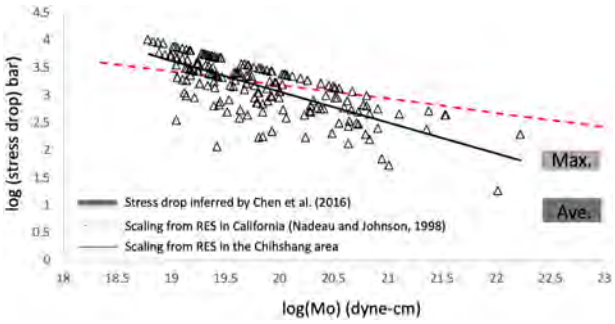

Figure 15. The stress drop versus seismic moment using the RES in eastern Taiwan. The open triangles denote the repeating events in the Chihshang area. The dashed line indicates the regression line from central SAF data by Nadeau and Johnson (1998). The box indicates a range of peak and averaged stress drop for two repeating events (M_L 4.3 and M_L 4.8) by Chen et al. (2016).

(1) This segment has been creeping with a stable slip rate of 4.3 cm/year at a depth of 15–25 km, and (2) the deep, creeping fault may extend further north along the NE-SW direction.

9.3. Magnitude and Spatial Distribution of Deep Slip on the LVF

Different geodetic measurements have been performed for the understanding of where and how the LVF creeps. The annual surveys of GPS, trilateration, and leveling data reveal a velocity discontinuity of 2–3 cm/year across the LVF, which is attributed to shallow aseismic creep (e.g., Lee & Angelier, 1993; Lee et al., 2005; Yu & Kuo, 2001; Yu & Liu, 1989). A rather shallow locked depth of 1.5 km was inferred for the Chihshang segment of LVF (Yu et al., 1990). Given that the no surface rupture was mapped during the 2003 M_L 6.4 event, the surface creeping zone is likely separated by a locked region from the aseismic slip at depth. Considering a shallowly dipping decollement, Hsu et al. (2003) inferred a creep rate of 2.8–3.3 cm/year at shallow depth (<8 km) of LVF and 4.8–6.2 cm/year at greater depth along the subhorizontal decollement. By adding the CRF into the modeling, Johnson et al. (2005) adopted viscoelastic rheology to infer a creep rate of 3.7–4.2 cm/year from surface to the depth of 20 km. Considering LVF, CRF, and west-dipping offshore fault, Huang et al. (2010) obtained 0.5- to 2.8-cm/year creep rate for the LVF, with the maximum fault slip occurring on the Chihshang segment at the depth of 15–20 km. The above creep rates inferred from different studies reveal a strong variation, which is mainly due to insufficient station coverage across the LVF.

Using PS-InSAR, the density of measurement can reach ~50 points per km^2 for higher spatial resolution of interseismic slip rate (Champenois et al., 2012). The velocity offsets across the LVF range from 1 to 3 cm/year along the radar line of sight. The deformation on the creeping segment of the LVF, Chihshang fault, is found to be localized in a wide zone of 1–2 km. It was not until Thomas et al. (2014) inverted the GPS and PS-InSAR data that an along-LVF fault coupling model was ready. They found that the majority of southern LVF is experiencing deep creep especially in the Chihshang segment, whereas northern LVF in the Linding and Ruisui segments is fully locked (Figure 1). The aseismic slip appears to be steady over time in the northmost Chihshang fault, where the slip rate is averaged as ~4 cm/year. In the middle of the Chihshang fault, the 2003 M_L 6.4 Chengkung earthquake is found to rupture a locked zone without propagating into the surrounding creeping area especially shallower than 7 km. The uppermost part of the fault, although well documented as a creeping zone, is found to respond differently to a large event (see figure 9 in Thomas et al., 2014), suggesting a strong along-strike variation of shallow creeping behavior and that the surface creep rate is a result of change in both seismic and aseismic slip at depth. However, at greater depth below the coseismic rupture of the Chengkung event, the preseismic, coseismic, and postseismic behavior is less certain due to poor resolution of inversions. This indicates that the understanding of along-dip variation of aseismic creep is still limited. The repeating earthquakes, although provide additional constraint on deep slip rate, are spatially limited to the depth of deeper than 7 km (minimum depth of RES on the Chihshang fault). The kinematic model combining geodetically derived surface deformation and observations of fault creep obtain from RES can be expected in the future.

9.4. Episodic Deep Slip on LVF

Episodic creep events have been studied under different tectonic settings. Using repeating earthquakes, the quasiperiodic creep pulsing was found to have a 2- to 3-year recurrence interval (Nadeau & McEvilly, 2004; Turner et al., 2015; Uchida et al., 2016). Such repetition is seen in different segments along the 175-km-long SAF, indicating an episodic change of creep rate from greater depth where the fault deformed more ductily (Nadeau & McEvilly, 2004). This repetition of extensive creep is also found in the northeastern Japan subduction zone. The dominant intervals of creep rate range from 1 to 6 years, coinciding with the timing of the clustered $M_L \geq 5$ earthquakes (Uchida et al., 2016). Given that the extensive creep events occurred few days before the $M_L \geq 5$ earthquakes, the accelerated creep is believed to have acted as a "trigger" for the mainshocks rather than having been triggered by the afterslip of the $M_L \geq 5$ events. Such quasiperiodic pulsing of the fault slip may be related to the slow slip events (SSE) rooted deeper below the seismogenic zone that undergo long-period aseismic loading processes (Marsan et al., 2013). The recurrence behavior

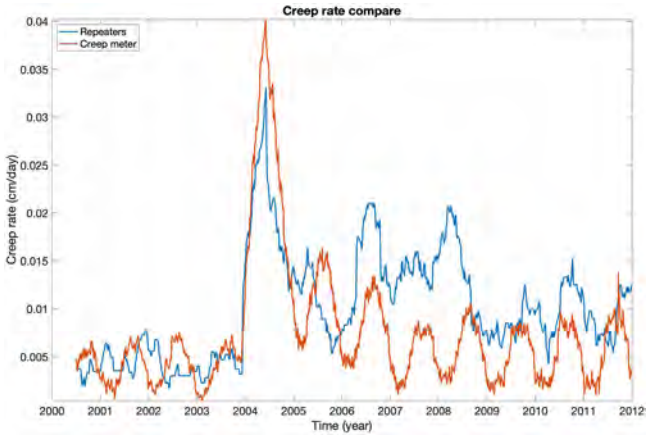

Figure 16. Time series of short-term slip rates from repeating earthquake and creepmeter results in the Chihshang area.

of the SSE is likely controlled by fault zone rheology and its elastic properties (Baumberger et al., 1994; Kaproth & Marone, 2013; Leeman et al., 2016, 2018).

The compaction-driven elevated pore fluid pressure and the following frictional dilation could be responsible for the episodic creep events along the SAF (Segall et al., 2010; Sleep & Blanpied, 1992). Such an effect produces heterogeneous distribution of creep, given that the rate of porosity reduction, the permeability, the rock material, and the geometrical irregularity of the fault surface are not the same across the entire fault. The elevated pore pressure and decreased permeability play an important role in SSE generation (Khoshmanesh & Shirzaei, 2018; Leclère et al., 2016) and can be detected by geodetic measurements. As addressed in Nadeau and McEvilly (2004), the variation of the deep creep rate correlates well with the geodetic measurements, and Turner et al. (2015) documented an approximately 2-year dominant periodic for both repeating earthquakes and InSAR data. Increase of the surface creep rate corresponds to elevation of the pore pressure and the reduction of effective normal stress, which may facilitate episodic aseismic creep at depth (Khoshmanesh & Shirzaei, 2018).

In Taiwan, the deep slip pulses have shorter recurrence intervals (~1 year) that can be compared with the surface creep histories. The on-site measurement of creepmeters straddling the surface traces of the Chihshang fault (Lee et al., 2001) provides the detailed evolution of surface creep to compare with. From creepmeters, the steady creep of 2.2–2.5 cm/year during the period of 1988–1998 was decreased to 1.5–1.8 cm/year in 2000–2003 (before the M_L 6.4 Chengkung event) and returned to 2.0 cm/year since 2007 (Mu et al., 2011). Before the 2003 M_L 6.4 mainshock, the surface creep measured by creepmeters shows strong seasonal fluctuations that is correlated with groundwater pressure variations measured at nearby wells (Chang et al., 2009; Lee et al., 2003, 2006). After the 2003 M_L 6.4 event, the surface creep increased several times greater than the preseismic level. These suggests that the surface creep on the Chihshang fault is characterized by (1) continuous creep with an averaged rate of ~2 cm/year, (2) small difference in creep rate between wet and dry seasons, and (3) preseismic, coseismic, and postseismic effect from the large earthquake (e.g., Chang et al., 2009; Lee et al., 2001, 2003, 2006; Mu et al., 2011; Thomas et al., 2014). The seasonal variation of the creepmeter data is explained by the ground water pressure variation at the wells close to the fault (Chang et al., 2009). However, the comparison between deep and surface creep variation in time (Figure 16) reveals a significant seasonal rhythm, where the creepmeter data seems to correlate well with the deep slip histories of the repeating events. This may suggest a common mechanism for surface and deep creep variation in time, either the stress applied to deep fault is from external sources from precipitation, or the episodic creep events from greater depth contribute to the surface creep.

Such annual variation is also seen in the tremor activity located west of the Chihshang fault, underneath the southern Central Range. Chen et al. (2018) found that tremor rhythm coincides with the rising of ocean tides, decreasing air pressure, low ground water levels, and minimal precipitation. By computing stresses from tidal and water storage changes, the greater than 4–5 kPa of pressure induced by annual water loading potentially has a greater influence on tremor activity, which is only a few kPa. As the tremors act as a proxy of SSE below the seismogenic zone, the deep creep events could be driven by the stress and pore pressure changes induced by the annual hydrologic load. We argued that the periodic stress perturbation from the hydrologic system may be the common mechanism that drives coherent slip pulses on the surface and at greater depths. The spatiotemporal distribution of repeating earthquakes in Figure S3 reveals several streaks that may indicate an upward migration, which is worth further investigation using clustering analysis and hypoDD relocation.

10. Conclusion

We documented 202 RES in eastern Taiwan from 2000 to 2011 with magnitudes ranging from 2.0 to 4.6. Of these 202 sequences, 187 were highly concentrated on the two opposite reverse faults: one being the east-dipping LVF and the other the west-dipping CRF. In this study, we explored the space and

time-dependent fault behavior of the LVF and CRF at depth and examined the methods of slip rate estimation for regional differences in deep creep rate.

Using the cumulative release smoothed over the summation of recurrence intervals for each individual quasiperiodic sequence and a geodetic data-derived interseismic slip rate, we obtained the averaged rupture area and determined the slip for individual repeating events. We refined the scaling relationship between the slip estimate and seismic moment as $\log d_i = -1.21+0.11 \log M_0$ and $\log d_i = -1.96+0.14 \log M_0$ for the creeping segments of the LVF and CRF, respectively.

Regional slip rates calculated from two groups of RES revealed strongly distinct behavior. Over 2004, the slip rate of the Chihshang segment of the LVF increased dramatically from 1.5 to 12.3 cm/year, showing a strong influence from the M_L 6.4 Chengkung earthquake that occurred on 10 December 2003. The acceleration decreased to 4.3 cm/year over 5 months after the mainshock and remained stable until the end of 2011. The surface deformation from the creepmeter, however, shows only a minor increase in the creep rate from 1.5–1.8 to 2.0 cm/year after the M_L 6.4 event, indicating a slip rate deficit of 2.3 cm/year accumulated above 7 km (i.e., the minimum depth of the RES). The RES in the Hualien area were separated into two groups: one corresponding to the CRF and the other corresponding to the extension of the LVF toward offshore. The slip rates on the creeping CRF were surprisingly high at 4.3 cm/year, showing no influence from nearby large earthquakes. This deep, long creep zone appears to extend in a northeasterly direction from 23.7°N to 24.4°N underneath the eastern flank of the Central Range. The other RES group associated with the LVF has a much slower slip rate of 3.5 cm/year.

A relatively high creep rate was found north of the Chihshang fault. Such quasiperiodic repetition of aseismic events exhibited an approximately 1-year interval, with the amplified creep rate occurring at the time of the 2003 M_L 6.4 earthquake. The aseismic slip pulsing in the southern segment, however, has a slightly longer interval of 2 years and was amplified by the 2006 M_L 6.0 earthquakes. The different arrival and periodicity of creep pulsing indicate that the demarcation of fault behavior may occur at a latitude of 23.0°N. On the other hand, the faster creep rate on the creeping CRF was found to be localized to the central segment (from 23.9°N to 24.2°N).

The short-term slip history from both areas reveals regularly recurring slip rate pulses. The semiannual cycle was found to coincide with the seasonable variation in the creepmeter data in the Chihshang area. Given that periodic stress perturbation from hydrological loads is able to produce stress change on a reverse fault of up to several kPa (Chen et al., 2018), this could be the common mechanism that drives coordinated slip pulses on the surface and at greater depths.

Acknowledgments
This work is supported through Taiwan MOST Grants MOST 108-2911-I-003-502 and MOST 108-2116-M-003-006-MY3. Seismic data are archived at the Central Weather Bureau Seismic Network (http://gdms.cwb.gov.tw/index.php), which is open for Taiwanese researcher. The broadband seismic data from Broadband Array in Taiwan for Seismology (BATS), however, can be freely accessed through http://bats.earth.sinica.edu.tw/Data/index.html. The repeating earthquake catalog conducted in this study can be freely downloaded and is now listed as supporting information and archived in public domain repository (the DOI of this data set is https://data.4tu.nl/repository/uuid:561970db--f717-4f54-8cd4-56c68d2f9c0a) to meet FAIR data standards. We wish to thank Pascal Bernard, an anonymous reviewer, and associate editor for their valuable comments. We also like to thank Chung-Hsiang Mu, Yaru Hsu, Roland Bürgmann, Ryne Turner, Erwan Pathier, and Gregory Shellnutt for their time and the invaluable discussions. We would like to thank Uni-edit (www.uni-edit.net) for editing and proofreading this manuscript.

References

Aki, K. (1966). Estimation of earthquake moment, released energy, and stress-strain drop from G-wave spectrum. *Bull Earthquake Res. Inst., Tokyo Univ.*, *44*, 73–88.

Angelier, J., Chu, H. T., & Lee, J. C. (1997). Shear concentration in a collision zone: Kinematics of the Chihshang fault as revealed by outcrop-scale quantification of active faulting, Longitudinal Valley, eastern Taiwan. *Tectonophysics*, *274*(1–3), 117–143. https://doi.org/10.1016/S0040-1951(96)00301-0

Angelier, J., Chu, H. T., Lee, J. C., & Hu, J. C. (2000). Active faulting and earthquake hazard: The case study of the Chihshang fault, Taiwan. *Journal of Geodynamics*, *29*(3–5), 151–185. https://doi.org/10.1016/S0264-3707(99)00045-9

Baumberger, T., Heslot, F., & Perrin, B. (1994). Crossover from creep to inertial motion in friction dynamics. *Nature*, *367*(6463), 544–546. https://doi.org/10.1038/367544a0

Beeler, N. M., Lockner, D. L., & Hickman, S. H. (2001). A simple stick-slip and creep-slip model for repeating earthquakes and its implication for microearthquakes at Parkfield. *Bulletin of the Seismological Society of America*, *91*(6), 1797–1804. https://doi.org/10.1785/0120000096

Biq, C. (1965). The East Taiwan Rift. *Pet. Geol. Taiwan*, *4*, 93–106.

Bürgmann, R., Schmidt, D., Nadeau, R. M., d'Alessio, M., Fielding, E., Manaker, D., et al. (2000). Earthquake potential along the northern Hayward fault, California. *Science*, *289*(5482), 1178–1182. https://doi.org/10.1126/science.289.5482.1178

Canitano, A., Hsu, Y. J., Lee, H. M., Linde, A. T., & Sacks, S. (2015). Near-field strain observations of the October 2013 Ruisui, Taiwan, earthquake: Source parameters and limits of very short-term strain detection. *Earth, Planets and Space*, *67*(1), 1–15. https://doi.org/10.1186/s40623-015-0284-1

Champenois, J., Fruneau, B., Pathier, E., Deffontaines, B., Lin, K. C., & Hu, J. C. (2012). Monitoring of active tectonic deformations in the Longitudinal Valley (Eastern Taiwan) using Persistent Scatterer InSAR method with ALOS PALSAR data. *Earth and Planetary Science Letters*, *337–338*, 144–155. https://doi.org/10.1016/j.epsl.2012.05.025

Chang, S. H., Wang, W. H., & Lee, J. C. (2009). Modelling temporal variation of surface creep on the Chihshang fault in eastern Taiwan with velocity-strengthening friction. *Geophysical Journal International*, *176*(2), 601–613. https://doi.org/10.1111/j.1365-246X.2008.03995.x

Chen, K. H., & Bürgmann, R. (2017). Creeping faults: Good news, bad news? *Reviews of Geophysics*, *55*, 282–286. https://doi.org/10.1002/2017RG000565

Chen, K. H., Chen, I., & Kim, A. (2016). Can slip heterogeneity be linked to earthquake recurrence? *Geophysical Research Letters*, *43*, 6916–6923. https://doi.org/10.1002/2016GL069516

Chen, K. H., Nadeau, R. M., & Rau, R. J. (2007). Towards a universal rule on the recurrence interval scaling of repeating earthquakes? *Geophysical Research Letters*, *34*. https://doi.org/10.1029/2007GL030554

Chen, K. H., Nadeau, R. M., & Rau, R. J. (2008). Characteristic repeating earthquakes in an arc-continent collision boundary zone: The Chihshang fault of eastern Taiwan. *Earth and Planetary Science Letters*, *276*(3–4), 262–272. https://doi.org/10.1016/j.epsl.2008.09.021

Chen, K. H., Rau, R. J., & Hu, J. C. (2009). Variability of repeating earthquake behavior along the Longitudinal Valley fault zone of eastern Taiwan. *Journal of Geophysical Research*, *114*. https://doi.org/10.1029/2007JB005518

Chen, T., & Lapusta, N. (2009). Scaling of small repeating earthquakes explained by interaction of seismic and aseismic slip in a rate and state fault model. *Journal of Geophysical Research*, *114*. https://doi.org/10.1029/2008JB005749

Chen, W. S., Wu, Y. M., Yeh, P. Y., Lai, Y. X., Ke, M. C., Ke, S. S., & Lin, Y. K. (2018). Seismogenic structures of the Eastern Taiwan collision zone. *Special Publication of the Central Geological Survey*, *33*, 123–155.

Chen, W. S., Yen, I. C., Fengler, K. P., Rubin, C. M., Yang, C. C., Yang, H. C., et al. (2007). Late Holocene paleoearthquake activity in the middle part of the Longitudinal Valley fault, eastern Taiwan. *Earth and Planetary Science Letters*, *264*(3–4), 420–437. https://doi.org/10.1016/j.epsl.2007.09.043

Cheng, S. N., Yeh, Y. T., & Yu, M. D. (1996). The 1951 Taitung earthquake in Taiwan. *Journal of the Geological Society of China*, *39*(3), 267–285.

Ching, K. E., Hsieh, M. L., Johnson, K. M., Chen, K. H., Rau, R. J., & Yang, M. (2011). Modern vertical deformation rates and mountain building in Taiwan from precise leveling and continuous GPS observations, 2000–2008. *Journal of Geophysical Research*, *116*. https://doi.org/10.1029/2011JB008242

Ching, K. E., Rau, R. J., Lee, J. C., & Hu, J. C. (2007). Contemporary deformation of tectonic escape in SW Taiwan from GPS observations, 1995–2005. *Earth and Planetary Science Letters*, *262*(3–4), 601–619. https://doi.org/10.1016/j.epsl.2007.08.017

Ching, K. E., Rau, R. J., & Zeng, Y. (2007). Coseismic source model of the 2003 Mw 6.8 Chengkung earthquake, Taiwan, determined from GPS measurements. *Journal of Geophysical Research*, *112*. https://doi.org/10.1029/2006JB004439

Chuang, R. Y., Johnson, K. M., Kuo, Y. T., Wu, Y. M., Chang, C. H., & Kuo, L. C. (2014). Active back thrust in the eastern Taiwan suture revealed by the 2013 Rueisuei earthquake: Evidence for a doubly vergent orogenic wedge? *Geophysical Research Letters*, *41*(10), 3464–3470. https://doi.org/10.1002/2014GL060097

Dominguez, L. A., Taira, T., & Santoyo, M. A. (2016). Spatiotemporal variations of characteristic repeating earthquake sequences along the Middle America Trench in Mexico. *Journal of Geophysical Research: Solid Earth*, *121*, 8855–8870. https://doi.org/10.1002/2016JB013242

Dreger, D., Nadeau, R. M., & Chung, A. (2007). Repeating earthquake finite source models: Strong asperities revealed on the San Andreas fault. *Geophysical Research Letters*, *34*. https://doi.org/10.1029/2007GL031353

Duverger, C., Lambotte, S., Bernard, P., Lyon-Caen, H., Deschamps, A., & Nercessian, A. (2018). Dynamics of microseismicity and its relationship with the active structures in the western Corinth Rift (Greece). *Geophysical Journal International*, *215*(1), 196–221. https://doi.org/10.1093/gji/ggy264

Hanks, T. C., & Kanamori, H. (1979). A moment magnitude scale. *Journal of Geophysical Research*, *84*(B5), 2348–2350. https://doi.org/10.1029/JB084iB05p02348

Harris, R. A. (2017). Large earthquakes and creeping faults. *Reviews of Geophysics*, *55*, 169–198. https://doi.org/10.1002/2016RG000539

Hsu, L., & Bürgmann, R. (2006). Surface creep along the Longitudinal Valley fault, Taiwan from InSAR measurements. *Geophysical Research Letters*, *33*. https://doi.org/10.1029/2005GL024624

Hsu, T. L. (1962). Recent faulting in the Longitudinal Valley of eastern Taiwan. *Memoir of Geological Society of China*, *1*, 95–102.

Hsu, Y. J., Simons, M., Yu, S. B., Kuo, L. C., & Chen, H. Y. (2003). A two-dimensional dislocation model for interseismic deformation of the Taiwan mountain belt. *Earth and Planetary Science Letters*, *211*(3–4), 287–294. https://doi.org/10.1016/S0012-821X(03)00203-6

Hsu, Y. J., Yu, S. B., & Chen, H. Y. (2009). Coseismic and postseismic deformation associated with the 2003 Chengkung, Taiwan, earthquake. *Geophysical Journal International*, *176*(2), 420–430. https://doi.org/10.1111/j.1365-246X.2008.04009.x

Hu, J. C., Cheng, L. W., Chen, H. Y., Wu, Y. M., Lee, J. C., Chen, Y. G., et al. (2007). Coseismic deformation revealed by inversion of strong motion and GPS data: The 2003 Chengkung earthquake in eastern Taiwan. *Geophysical Journal International*, *169*(2), 667–674. https://doi.org/10.1111/j.1365-246X.2007.03359.x

Huang, K. C., Kao, H., Wu, Y. M. (2000). The determination of ML-MW in Taiwan. *In 8th Annual Meeting of Geophysical Society of China*, pp. 193–201. in Chinese.

Huang, W. J., Johnson, K. M., Fukuda, J., & Yu, S. B. (2010). Insights into active tectonics of eastern Taiwan from analyses of geodetic and geologic data. *Journal of Geophysical Research*, *115*. https://doi.org/10.1029/2008JB006208

Igarashi, T., Matsuzawa, T., & Hasegawa, A. (2003). Repeating earthquakes and interplate aseismic slip in the northeastern Japan subduction zone. *Journal of Geophysical Research*, *108*(B5). https://doi.org/10.1029/2002jb001920

Johnson, K. M., Segall, P., & Yu, S. B. (2005). A viscoelastic earthquake cycle model for Taiwan. *Journal of Geophysical Research*, *110*, 1–15. https://doi.org/10.1029/2004JB003516

Kanamori, H., & Anderson, D. L. (1975). Theoretical basis of some empirical relations in seismology. *Bulletin of the Seismological Society of America*, *65*(5), 1073–1095.

Kaproth, B. M., & Marone, C. (2013). Slow earthquakes, preseismic velocity changes, and the origin of slow frictional stick-slip. *Science*, *341*(6151), 1229–1232. https://doi.org/10.1126/science.1239577

Khoshmanesh, M., & Shirzaei, M. (2018). Episodic creep events on the San Andreas fault caused by pore pressure variations. *Nature Geoscience*, *11*(8), 610–614. https://doi.org/10.1038/s41561-018-0160-2

Khoshmanesh, M., Shirzaei, M., & Nadeau, R. M. (2015). Time-dependent model of aseismic slip on the central San Andreas fault from InSAR time series and repeating earthquakes. *Journal of Geophysical Research: Solid Earth*, *120*. 6658–6679. https://doi.org/10.1002/2015JB012039

Leclère, H., Faulkner, D., Wheeler, J., & Mariani, E. (2016). Permeability control on transient slip weakening during gypsum dehydration: Implications for earthquakes in subduction zones. *Earth and Planetary Science Letters*, *442*, 1–12. https://doi.org/10.1016/j.epsl.2016.02.015

Lee, J. C., & Angelier, J. (1993). Location of active deformation and geodetic data analyses: An example of the Longitudinal Valley Fault, Taiwan. *Bull. Soc. Geol. France*, *164*(4), 533–570.

Lee, J. C., Angelier, J., Chu, H. T., Hu, J. C., Jeng, F. S., & Rau, R. J. (2003). Active fault creep variations at Chihshang, Taiwan, revealed by creep meter monitoring, 1998–2001. *Journal of Geophysical Research*, *108*(B11). https://doi.org/10.1029/2003jb002394

Lee, J. C., Angelier, J., Chu, H. T., Hu, J. C., & Jeng, F. S. (2001). Continuous monitoring of an active fault in a plate suture zone: A creepmeter study of the Chihshang fault, eastern Taiwan. *Tectonophysics*, *333*(1–2), 219–240. https://doi.org/10.1016/S0040-1951(00)00276-6

Lee, J. C., Angelier, J., Chu, H. T., Hu, J. C., & Jeng, F. S. (2005). Monitoring active fault creep as a tool in seismic hazard mitigation. Insights from creepmeter study at Chihshang, Taiwan. *Comptes Rendus Geoscience*, *337*(13), 1200–1207. https://doi.org/10.1016/j.crte.2005.04.018

Lee, J. C., Chu, H. T., Angelier, J., Hu, J. C., Chen, H. Y., & Yu, S. B. (2006). Quantitative analysis of surface coseismic faulting and post-seismic creep accompanying the 2003, Mw = 6.5, Chengkung earthquake in eastern Taiwan. *Journal of Geophysical Research*, *111*. https://doi.org/10.1029/2005JB003612

Lee, J. C., Jeng, F. S., Chu, H. T., Angelier, J., & Hu, J. C. (2000). A rod-type creepmeter for measurement of displacement in active fault zone. *Earth, Planets and Space*, *52*(5), 321–328. https://doi.org/10.1186/BF03351643

Lee, S. J., Huang, H. H., Shyu, J. B. H., Yeh, T. Y., & Lin, T. C. (2014). Numerical earthquake model of the 31 October 2013 Ruisui, Taiwan, earthquake: Source rupture process and seismic wave propagation. *Journal of Asian Earth Sciences*, *96*, 374–385. https://doi.org/10.1016/j.jseaes.2014.09.020

Leeman, J. R., Marone, C., & Saffer, D. M. (2018). Frictional mechanics of slow earthquakes. *Journal of Geophysical Research: Solid Earth*, *123*, 7931–7949. https://doi.org/10.1029/2018JB015768

Leeman, J. R., Saffer, D. M., Scuderi, M. M., & Marone, C. (2016). Laboratory observations of slow earthquakes and the spectrum of tectonic fault slip modes. *Nature Communications*, *7*. https://doi.org/10.1038/ncomms11104

Liu, T. K., Chen, Y. G., Chen, W. S., & Jiang, S. H. (2000). Rates of cooling and denudation of the early Penglai orogeny, Taiwan, as assessed by fission-track constraints. *Tectonophysics*, *320*(1), 69–82. https://doi.org/10.1016/S0040-1951(00)00028-7

Malservisi, R., Furlong, K. P., & Gans, C. R. (2005). Microseismicity and creeping faults: Hints from modeling the Hayward fault, California (USA). *Earth and Planetary Science Letters*, *234*(3–4), 421–435. https://doi.org/10.1016/j.epsl.2005.02.039

Marsan, D., Reverso, T., Helmstetter, A., & Enescu, B. (2013). Slow slip and aseismic deformation episodes associated with the subducting Pacific plate offshore Japan, revealed by changes in seismicity. *Journal of Geophysical Research E: Planets*, *118*, 4900–4909. https://doi.org/10.1002/jgrb.50323

McLaskey, G. C., & Kilgore, B. D. (2013). Foreshocks during the nucleation of stick-slip instability. *Journal of Geophysical Research: Solid Earth*, *118*, 2982–2997. https://doi.org/10.1002/jgrb.50232

Mu, C. H., Angelier, J., Lee, J. C., Chu, H. T., & Dong, J. J. (2011). Structure and Holocene evolution of an active creeping thrust fault: The Chihshang fault at Chinyuan (Taiwan). *Journal of Structural Geology*, *33*(4), 743–755. https://doi.org/10.1016/j.jsg.2011.01.015

Nadeau, R. M., & Johnson, L. R. (1998). Seismological studies at Parkfield VI: Moment release rates and estimates of source parameters for small repeating earthquake. *Bulletin of the Seismological Society of America*, *88*(3), 790–814.

Nadeau, R. M., & McEvilly, T. V. (1999). Fault slip rates at depth from recurrence intervals of repeating microearthquakes. *Science*, *285*(5428), 718–721. https://doi.org/10.1126/science.285.5428.718

Nadeau, R. M., & McEvilly, T. V. (2004). Periodic pulsing of characteristic microearthquakes on the San Andreas fault. *Science*, *303*(5655), 220–222. https://doi.org/10.1126/science.1090353

Rau, R. J., Chen, K. H., & Ching, K. E. (2007). Repeating earthquakes and seismic potential along the northern Longitudinal Valley fault of eastern Taiwan. *Geophysical Research Letters*, *34*. https://doi.org/10.1029/2007GL031622

Rau, R. J., Ching, K. E., Hu, J. C., & Lee, J. C. (2008). Crustal deformation and block kinematics in transition from collision to subduction: Global positioning system measurements in northern Taiwan, 1995–2005. *Journal of Geophysical Research*, *113*. https://doi.org/10.1029/2007JB005414

Sammis, C. G., & Rice, J. R. (2001). Repeating earthquakes as low-stress-drop events at a border between locked and creeping fault patches. *Bulletin of the Seismological Society of America*, *91*(3), 532–537. https://doi.org/10.1785/0120000075

Segall, P., Rubin, A. M., Bradley, A. M., & Rice, J. R. (2010). Dilatant strengthening as a mechanism for slow slip events. *Journal of Geophysical Research*, *115*. https://doi.org/10.1029/2010JB007449

Shyu, J. B. H., Sieh, K., Chen, Y. G., & Chung, L. H. (2006). Geomorphic analysis of the Central Range fault, the second major active structure of the Longitudinal Valley suture, eastern Taiwan. *Bulletin of the Geological Society of America*, *118*(11–12), 1447–1462. https://doi.org/10.1130/B25905.1

Sleep, N. H., & Blanpied, M. L. (1992). Creep, compaction and the weak rheology of major faults. *Nature*, *359*(6397), 687–692. https://doi.org/10.1038/359687a0

Templeton, D. C., Nadeau, R. M., & Bürgmann, R. (2008). Behavior of repeating earthquake sequences in Central California and the implications for subsurface fault creep. *Bulletin of the Seismological Society of America*, *98*(1), 52–65. https://doi.org/10.1785/0120070026

Thomas, M. Y., Avouac, J. P., Champenois, J., Lee, J. C., & Kuo, L. C. (2014). Spatiotemporal evolution of seismic and aseismic slip on the Longitudinal Valley fault, Taiwan. *Journal of Geophysical Research: Solid Earth*, *119*, 5114–5139. https://doi.org/10.1002/2013JB010603

Thomas, M. Y., Avouac, J.-P., & Lapusta, N. (2017). Rate-and-state friction properties of the Longitudinal Valley fault from kinematic and dynamic modeling of seismic and aseismic slip. *Journal of Geophysical Research: Solid Earth*, *122*. https://doi.org/10.1002/2016JB013615

Tung, H., Chen, H. Y., Hsu, Y. J., Hu, J. C., Chang, Y. H., & Kuo, Y. T. (2019). Triggered slip on multifaults after the 2018 Mw 6.4 Hualien earthquake by continuous GPS and InSAR measurements. *Terrestrial, Atmospheric and Oceanic Sciences*, *30*(3), 285–300. https://doi.org/10.3319/tao.2019.04.03.01

Turner, R. C., Shirzaei, M., Nadeau, R. M., & Bürgmann, R. (2015). Slow and go: Pulsing slip rates on the creeping section of the San Andreas fault. *Journal of Geophysical Research: Solid Earth*, *120*, 5940–5951. https://doi.org/10.1002/2015JB011998

Uchida, N., Iinuma, T., Nadeau, R. M., Bürgmann, R., & Hino, R. (2016). Periodic slow slip triggers megathrust zone earthquakes in northeastern Japan. *Science*, *351*(6272), 488–492. https://doi.org/10.1126/science.aad3108

Uchida, N., Matsuzawa, T., Hasegawa, A., & Igarashi, T. (2003). Interplate quasi-static slip off Sanriku, NE Japan, estimated from repeating earthquakes. *Geophysical Research Letters*, *30*(15). https://doi.org/10.1029/2003GL017452

Vidale, J. E., & Shearer, P. M. (2006). A survey of 71 earthquake bursts across southern California: Exploring the role of pore fluid pressure fluctuations and aseismic slip as drivers. *Journal of Geophysical Research*, *111*. https://doi.org/10.1029/2005JB004034

Wen, Y. Y., Yen, Y. T., Wen, S., Lee, S. J., Kuo, C. H., & Lin, Y. Y. (2016). Hybrid ground motion simulation for the 2013 ML 6.4 Ruisui, Taiwan earthquake. *Terrestrial, Atmospheric and Oceanic Sciences*, *27*(3), 407. https://doi.org/10.3319/tao.2015.10.30.01(tem)

Wu, Y. M., Chen, Y. G., Chang, C. H., Chung, L. H., Teng, T. L., Wu, F. T., & Wu, C. F. (2006). Seismogenic structure in a tectonic suture zone: With new constraints from 2006 Mw6.1 Taitung earthquake. *Geophysical Research Letters*, *33*. https://doi.org/10.1029/2006GL027572

Wu, Y. M., Shyu, J. B. H., Chang, C. H., Zhao, L., Nakamura, M., & Hsu, S. K. (2009). Improved seismic tomography offshore northeastern Taiwan: Implications for subduction and collision processes between Taiwan and the southernmost Ryukyu. *Geophysical Journal International*, *178*, 1042–1054. https://doi.org/10.1111/j.1365-246X.2009.04180.x

Yen, J. Y., Lu, C. H., Dorsey, R. J., Kuo-Chen, H., Chang, C. P., Wang, C. C., et al. (2019). Insights into seismogenic deformation during the 2018 Hualien, Taiwan, earthquake sequence from InSAR, GPS, and modeling. *Seismological Research Letters*, *90*(1), 78–87. https://doi.org/10.1785/0220180228

Yu, S. B., Chen, H. Y., & Kuo, L. C. (1997). Velocity field of GPS stations in the Taiwan area. *Tectonophysics*, *274*(1–3), 41–59. https://doi.org/10.1016/S0040-1951(96)00297-1

Yu, S. B., Jackson, D. D., Yu, G. K., & Liu, C. C. (1990). Dislocation model for crustal deformation in the Longitudinal Valley area, eastern Taiwan. *Tectonophysics*, *183*(1–4), 97–109. https://doi.org/10.1016/0040-1951(90)90190-J

Yu, S. B., & Kuo, L. C. (2001). Present-day crustal motion along the Longitudinal Valley fault, eastern Taiwan. *Tectonophysics*, *333*(1–2), 199–217. https://doi.org/10.1016/S0040-1951(00)00275-4

Yu, S. B., & Liu, C. C. (1989). Fault creep on the central segment of the Longitudinal Valley fault, eastern Taiwan. *Proc.tt Geol. Soc. China*, *32*, 209–231.

Yu, W. C. (2013). Shallow-focus repeating earthquakes in the tonga-kermadec-vanuatu subduction zones. *Bulletin of the Seismological Society of America*, *103*(1), 463–486. https://doi.org/10.1785/0120120123